

1 **Specific glucoside transporters influence septal structure and function in the**
 2 **filamentous, heterocyst-forming cyanobacterium *Anabaena* sp. strain PCC**
 3 **7120**

4
 5 Mercedes Nieves-Mori3n¹, Sigal Lechno-Yossef², Roc3o L3pez-Igual^{1*}, Jos3 E. Fr3as¹, Vicente
 6 Mariscal¹, Dennis J. N3rnberg³, Conrad W. Mullineaux⁴, C. Peter Wolk², and Enrique Flores^{1#}

7
 8 ¹Instituto de Bioqu3mica Vegetal y Fotos3ntesis, CSIC and Universidad de Sevilla, Am3rico
 9 Vespucio 49, E-41092 Seville, Spain; ²MSU-DOE Plant Research Laboratory, Michigan State
 10 University, East Lansing, Michigan 48824, USA; ³Department of Life Sciences, Imperial
 11 College London, London SW7 2AZ, United Kingdom; ⁴School of Biological and Chemical
 12 Sciences, Queen Mary University of London, Mile End Road, London E1 4NS, United
 13 Kingdom.

14
 15 *Running head:* Glucoside transporters in *Anabaena*

16
 17 #Address correspondence to Enrique Flores, eflores@ibvf.csic.es.

18
 19 *Present address: Institut Pasteur, Unit3 Plasticit3 du G3nome Bact3rien, D3partement G3nomes
 20 et G3n3tique, CNRS, Unit3 Mixte de Recherche 3525, F-75015 Paris, France

21
 22 *Key words:* Cyanobacteria; Glucoside transport; Heterocyst; Intercellular diffusion; Membrane
 23 transporters.

24 **ABSTRACT**

25 When deprived of combined nitrogen, some filamentous cyanobacteria contain two cell types: vegetative
26 cells that fix CO₂ through oxygenic photosynthesis and heterocysts that are specialized in N₂ fixation. In
27 the diazotrophic filament, the vegetative cells provide the heterocysts with reduced carbon (mainly in the
28 form of sucrose) and heterocysts provide the vegetative cells with combined nitrogen. Septal junctions
29 traverse peptidoglycan through structures known as nanopores, and appear to mediate intercellular
30 molecular transfer that can be traced with fluorescent markers, including the sucrose analog esculin (a
31 coumarin glucoside) that is incorporated into the cells. Uptake of esculin by the model heterocyst-forming
32 cyanobacterium *Anabaena* sp. strain PCC 7120 was inhibited by the α -glucosides sucrose and maltose.
33 Analysis of *Anabaena* mutants identified components of three glucoside transporters that move esculin
34 into the cells: GlsC (Alr4781) and GlsP (All0261) are, respectively, an ATP-binding subunit and a
35 permease subunit of two different ABC transporters, and HepP (All1711) is a major facilitator
36 superfamily (MFS) protein that was shown previously to be involved in formation of the heterocyst
37 envelope. Transfer of fluorescent markers (especially calcein) between vegetative cells of *Anabaena* was
38 impaired by mutation of glucoside transporter genes. GlsP and HepP interact in bacterial two-hybrid
39 assays with the septal junction-related protein SepJ, and GlsC was found to be necessary for formation of
40 a normal number of septal peptidoglycan nanopores and for normal subcellular localization of SepJ.
41 Therefore, beyond their possible role in nutrient uptake in *Anabaena*, glucoside transporters influence the
42 structure and function of septal junctions.

43

44 **IMPORTANCE**

45 Heterocyst-forming cyanobacteria have the ability to perform oxygenic photosynthesis and to assimilate
46 atmospheric CO₂ and N₂. These organisms grow as filaments that fix these gases specifically in vegetative
47 cells and heterocysts, respectively. For the filaments to grow, these types of cells exchange nutrients
48 including sucrose, which serves as a source of reducing power and of carbon skeletons for the heterocysts.
49 Movement of sucrose between cells in the filament takes place through septal junctions and has been
50 traced with a fluorescent sucrose analog, esculin, that can be taken up by the cells. We here identified α -
51 glucoside transporters of *Anabaena* that mediate uptake of esculin and, notably, influence septal structure
52 and the function of septal junctions.

53

54 INTRODUCTION

55 Filamentous cyanobacteria of the orders Nostocales and Stigonematales fix atmospheric nitrogen in
56 specialized cells called heterocysts (1). Heterocysts are formed from vegetative cells when the filaments
57 of those cyanobacteria lack a source of combined nitrogen (2). The heterocysts provide the vegetative
58 cells with fixed nitrogen, and the vegetative cells, which fix carbon dioxide through oxygenic
59 photosynthesis, provide the heterocysts with reduced carbon (3). Substances exchanged between the two
60 cell types include regulators such as PatS- and HetN-derived peptides and nutrients including amino acids
61 and sugars (4). In the model heterocyst-forming cyanobacterium *Anabaena* sp. strain PCC 7120 (hereafter
62 *Anabaena*) grown in the absence of combined nitrogen, heterocysts constitute about 10% of the cells and
63 are distributed with a semi-regular pattern along the filament (2). This implies that one heterocyst feeds
64 more than one vegetative cell with fixed nitrogen. Two routes have been considered for intercellular
65 molecular transfer, the continuous periplasm of the filament (5, 6) and cell-cell joining structures (7), now
66 termed septal junctions (8-10). The latter would represent a kind of symplasmic route (11) implying
67 intercellular transfer between vegetative cells as well as between heterocysts and vegetative cells.

68 Proteins SepJ, FraC and FraD that are located at the cell poles in the intercellular septa of the
69 filaments of *Anabaena* are integral membrane proteins (12, 13). SepJ and FraD have predicted extra-
70 membrane domains that appear to reside in the periplasm (10, 14-16). Intercellular molecular exchange in
71 the cyanobacterial filament can be traced with fluorescent markers including calcein, 5-
72 carboxyfluorescein (5-CF) and esculin, and transfer has been found to be impaired in inactivated mutants
73 of *sepJ*, *fraC* and *fraD* (7, 14, 17, 18). Additionally, perforations (termed nanopores) that have been
74 observed in septal peptidoglycan disks from heterocyst-forming cyanobacteria (19) are present at
75 decreased numbers in those mutants (18). Structures observed by electron tomography of *Anabaena* that
76 have been termed “channels” (20) likely correspond to the nanopores. SepJ, FraC and FraD appear to
77 contribute to the formation of cell-cell joining structures (septal junctions) that traverse the septal
78 peptidoglycan through the nanopores. Differential impairment in the transfer of calcein and 5-CF in the

79 *sepJ* and *fraC-fraD* mutants has suggested that two types of septal junction complexes exist, one related
80 to SepJ and another related to FraCD (14).

81 Sucrose appears to be a quantitatively important metabolite transferred from vegetative cells to
82 heterocysts (21-25). Intercellular transfer of sucrose has been probed in *Anabaena* using esculin (6,7-
83 dihydroxycoumarin β -D-glucoside), a fluorescent analog of this sugar (18). Esculin is taken up into the
84 cells by a mechanism that can be inhibited by the presence of sucrose. Once inside the cells, esculin can
85 be transferred cell-to-cell in the filament by diffusion through the septal junctions (18, 26). Thus, septal
86 junctions are functionally analogous to the gap junctions of metazoans (18, 26).

87 In this work, we addressed the transporters that are involved in esculin uptake in *Anabaena* and
88 their role, if any, in intercellular molecular transfer. The genome of *Anabaena* contains several open
89 reading frames predicted to encode components of sugar transporters (27). We have identified three genes
90 that are involved in uptake of esculin, two that encode components of two different ABC uptake
91 transporters and one that encodes a Major Facilitator Superfamily (MFS) transporter. We also found that
92 the three identified glucoside transporters influence intercellular molecular exchange in *Anabaena*. One of
93 the ABC transporter components, an ATP-binding subunit, is needed for the correct subcellular
94 localization of SepJ, and the two other transporters appear to affect SepJ function.

95

96 MATERIALS AND METHODS

97 **Strains and growth conditions.** *Anabaena* sp. strain PCC 7120 and derivative strains (described in Table
98 S1) were grown in BG11 medium modified to contain ferric citrate instead of ferric ammonium citrate
99 (28) or BG11₀ medium (BG11 further modified by omission of NaNO₃) at 30°C in the light (ca. 25-30
100 $\mu\text{mol photons m}^{-2} \text{ s}^{-1}$), in shaken (100 r.p.m.) liquid cultures. For tests on solid medium, media BG11 or
101 BG11₀ were solidified with 1% (w/v) Difco Bacto agar. For isolation of the *glsC* (*alr4781*), *glsP*
102 (*all0261*) and *glsC glsP* mutants, *Anabaena* was grown, with shaking, in flask cultures of AA/8 liquid
103 medium with nitrate (29), or in medium AA with nitrate solidified with 1.2% (w/v) purified (Difco) Bacto

104 agar (29) at 30°C and illuminated as above. When appropriate, antibiotics were added to the
105 cyanobacterial cultures at the following concentrations: in liquid cultures—streptomycin sulfate (Sm), 2-5
106 $\mu\text{g ml}^{-1}$; spectinomycin dihydrochloride pentahydrate (Sp), 2-5 $\mu\text{g ml}^{-1}$; erythromycin (Em), 5 $\mu\text{g ml}^{-1}$; and
107 neomycin sulfate (Nm), 5-25 $\mu\text{g ml}^{-1}$; and in solid media—Sm, 5-10 $\mu\text{g ml}^{-1}$; Sp, 5-10 $\mu\text{g ml}^{-1}$; Em, 5-10
108 $\mu\text{g ml}^{-1}$; and Nm, 30-40 $\mu\text{g ml}^{-1}$. Chlorophyll *a* (Chl) content of cultures was determined by the method of
109 Mackinney (30).

110 *Escherichia coli* strains were grown in LB medium, supplemented when appropriate with
111 antibiotics at standard concentrations (31). *E. coli* strains DH5 α or DH5 α MCR were used for plasmid
112 constructions. *E. coli* strains DH5 α or ED8654 bearing a conjugative plasmid, and strains HB101 or
113 DH5 α MCR bearing a methylase-encoding helper plasmid and the cargo plasmid, were used for
114 conjugation with *Anabaena*, unless stated otherwise (32).

115 **Construction of *Anabaena* mutant strains.** The *alr4781* (*glsC*) mutant, DR3912a, was
116 generated by a di-parental mating between *Anabaena* and DH5 α MCR carrying pRL443, pRL3857a and
117 pRL3912a (plasmids described in Table S1). The single recombinant was selected on Em, tested for
118 sucrose sensitivity, and then went through a sucrose selection cycle, as described by Cai and Wolk (33),
119 for selection of the double recombinant (Fig. S1). Similarly, a double recombinant deletion mutant of
120 *all0261* (*glsP*), DR3915 (Fig. S1), was generated by mating between *Anabaena* and DH5 α MCR carrying
121 pRL443, pRL3857a and pRL3915. Because DR3912a and DR3915 carry the same antibiotic resistance
122 marker (Sm^R Sp^R), a new plasmid, pRL3985a, was constructed for creation of the *glsC glsP* double
123 mutant (Fig. S1). In this case, pRL3985a was introduced into DR3912a by conjugation, and the mutant
124 was selected as described above.

125 For complementation of the *glsC* mutant (DR3912a), a fragment containing ORF *alr4781* and 202
126 bp of upstream and 49 bp of downstream DNA was amplified using *Anabaena* DNA as template and
127 primers alr4781-3 and alr4781-4 (oligodeoxynucleotide primers are described in Table S1). The PCR
128 product was cloned into vector pSpark I producing pCSMN21. This construct was verified by sequencing
129 and transferred as a BamHI fragment to pRL25C (34) digested with the same enzyme producing

130 pCSMN22. This plasmid was transferred to DR3912a by conjugation. Clones resistant to Sm, Sp and Nm
131 were isolated and their genetic structure was verified by PCR with primers alr4781-3 and alr4781-4 (Fig.
132 S2). This strain was named CSMN11. For complementation of the *glsP* mutant (DR3915), a fragment
133 containing ORF *all0261* and 103 bp of upstream and 40 bp of downstream DNA was amplified using
134 *Anabaena* DNA as template and primers all0261-3 and all0261-4. The PCR product was cloned into
135 pSpark I producing pCSMN19, which was confirmed by sequencing and transferred as a BamHI fragment
136 to pRL25C digested with BamHI producing pCSMN20. This plasmid was transferred to DR3915 by
137 conjugation. Clones resistant to Sm, Sp and Nm were isolated and their genetic structure was verified by
138 PCR with primers all0261-3 and all0261-4 (Fig. S2). This strain was named CSMN12.

139 For inactivation of *alr3705*, an internal fragment of 560 bp was amplified by PCR using
140 *Anabaena* DNA as template and primers alr3705-1 (bearing a BamHI site in its 5' end) and alr3705-2.
141 The amplified fragment was cloned into pMBL-T (<http://www.molbiolab.es/uploads/phpgSgmue.pdf>;
142 Dominion MBL, Spain) and transferred as a BamHI-ended fragment (the second BamHI site is from the
143 vector multiple cloning site) to BamHI-digested pCSV3 (35) producing pCSRL49. This plasmid was
144 transformed into *E. coli* HB101 (pRL623) and transferred to *Anabaena* and to *hepP* (*all1711*) mutant
145 strain FQ163 (36) by conjugation with selection for Sm^R Sp^R (because FQ163 is itself Nm^R Sm^R
146 bleomycin^R, in this case effective selection is only for Sp^R). Clones that had incorporated pCSRL49 by
147 single recombination were selected for further study and named strain CSRL15 (wild-type background)
148 and CSMN3 (*hepP* background) (Fig. S3).

149 To prepare an *Anabaena* strain producing a fusion of the GFP to GlcC, a 950-bp DNA fragment
150 from the 3' region of *glsC* (*alr4781*) was amplified using *Anabaena* DNA as template and primers
151 alr4781-5 and alr4781-6. The 950-bp PCR product was cloned into pSpark I producing pCSMN23. This
152 construct was validated by sequencing and transferred to SacI-XhoI-digested pRL277 (37) as a SacI-NheI
153 fragment together with NheI-SalI-digested *gfp-mut2* (38), producing pCSMN24, in which the *gfp-mut2*
154 gene is fused to *glsC*. pCSMN24 was transferred to *Anabaena* by conjugation. Clones resistant to Sm and
155 Sp were selected and their genetic structure was verified by PCR with primer pairs alr4781-3/gfp-5 and

156 alr4781-3/alr4781-4. This strain was named CSMN13 (Fig. S4). To prepare an *Anabaena* strain
157 producing a fusion of the GFP to GlsP, a 482-bp DNA fragment from the 3' region of *glsP* (*all0261*) was
158 amplified using *Anabaena* DNA as template and primers all0261-6 and all0261-5. The PCR product, a
159 SacI-NheI fragment, was inserted together with NheI-SalI digested *gfp-mut2* into SacI-XhoI-digested
160 pRL277 (37), producing pCSMN25, which bears a fusion of the *all0261* coding sequence to the *gfp-mut2*
161 gene. This construct was verified by sequencing and transferred to *Anabaena* by conjugation. Clones
162 resistant to Sm and Sp were isolated, and integration of the *glsP-gfp* construct was verified by PCR using
163 primer pairs all0261-4/gfp-5 and all0261-3/all0261-4. This strain was named CSMN15 (Fig. S4).

164 To study the effect of inactivation of transporter genes on the localization of SepJ-GFP, Nm^R
165 plasmid pCSVT22 bearing *sepJ-gfp* (13) was transferred to strains DR3912a (*alr4781::C.S3*) and
166 DR3915 (*all0261::C.S3*) by conjugation. Similarly, the Sm^RSp^R plasmid pCSAM137 bearing *sepJ-gfp*
167 (12) was transferred to FQ163 (*hepP::Tn5-1063*; 36). The genetic structure of selected clones bearing
168 *sepJ-gfp* fusions was studied by PCR with DNA from those clones and primer pair alr2338-3/gfp-5 to test
169 recombination in the correct genomic location (*sepJ*). We also verified the mutant background in the
170 exconjugants using the following primer pairs: for *alr4781*, alr4781-3/alr4781-4; for *all0261*, all0261-
171 3/all0261-4; and for *hepP*, all1711-3/all1711-4 (Fig. S5). Clones bearing the *sepJ-gfp* fusion were named
172 strain CSMN9 (*alr4781* background), CSMN10 (*all0261* background) and CSMN16 (*hepP* background).

173 **RT-qPCR.** RNA was isolated as described (36) from 50 to 100 ml of shaken *Anabaena* cultures.
174 RNA was treated with Ambion® TURBO DNA-free™ DNase according to the manufacturer's protocol.
175 Three independent RNA samples were analyzed from each strain (the wild type and the complemented
176 *glsC* and *glsP* strains) and three technical replicas were carried out for each sample. RNA (200 ng) was
177 reverse-transcribed using QuantiTect® Reverse Transcription Kit (Qiagen) with random primers as
178 indicated by standard protocols of the manufacturer. Quantitative real-time PCR was performed on an
179 *iCycler iQ Real Time PCR Detection System* equipped with the software *iCycler iQ v 3.0* from BioRad.
180 PCR amplification was performed in a 20-μl reaction mix according to standard protocols of
181 SensiFAST™ SYBR and Fluorescein Kit (Bioline). The Q-PCR conditions were as follows: 1 cycle at 95

182 °C for 2 min, 30 cycles of: 95 °C for 15 s, 67.5 °C for 20 s and 72 °C for 30 s. PCR products were checked
183 by a single-peak melting curve. The threshold cycle (Ct) of each gene was determined and normalized to
184 those of reference genes *ispD* (*all5167*) and *dxs* (*alr0599*), to obtain ΔC_t values from each sample.
185 Relative gene expression was calculated using the $2^{-\Delta\Delta C_t}$ method (39), and the data presented correspond
186 to the average of data obtained with each reference gene. The following primer pairs were used: all0261-
187 11/all0261-12, alr4781-9/alr4781-10, all5167-1/all5167-2 and alr0599-1/alr0599-2 (Table S1).

188 **Uptake of esculin.** *Anabaena* strains grown in BG11 medium—with antibiotics for the
189 mutants—were harvested by centrifugation, washed three times with BG11 or BG11₀ medium without
190 antibiotics and incubated for 18 h in the same medium under culture conditions. Cells were harvested,
191 washed and resuspended in the corresponding growth medium supplemented with 10 mM HEPES-NaOH
192 buffer (pH 7, unless indicated otherwise), and 1 mM of the indicated sugar in the experiment described in
193 Fig. 3. Assays of uptake were started by addition of esculin hydrate (Sigma-Aldrich) at 100 μ M, and
194 suspensions were incubated at 30°C in the light ($\sim 170 \mu\text{mol photons m}^{-2} \text{ s}^{-1}$) for up to 70 min. One-ml
195 samples were withdrawn and filtered. Cells on the filters were washed with 10 mM HEPES-NaOH buffer
196 of the same pH used in the assay and were resuspended in 2 ml of 10 mM HEPES-NaOH buffer (pH 7).
197 Fluorescence of the resulting cell suspension was measured in a Varian Cary Eclipse Fluorescence
198 Spectrophotometer (excitation 360 ± 10 nm; emission 462 ± 10 nm). Esculin solutions in the same buffer
199 (pH 7) were used as standards. Significance in the differences of uptake between strains (as well as in
200 other parameters investigated in this work) was assessed by unpaired Student's *t* tests, assuming a normal
201 distribution of the data. Data sets with values of $P < 0.05$ are considered significant.

202 **Growth curves and nitrogenase activity.** The growth rate constant ($\mu = [\ln 2]/t_d$, where t_d is the
203 doubling time) was calculated from the increase in OD_{750 nm} of shaken liquid cultures. Cultures were
204 inoculated with an amount of cells giving an OD_{750 nm} of about 0.05 (light path, 1 cm) and grew
205 logarithmically until reaching an OD_{750 nm} of about 0.8-0.9. The suspensions of filaments were carefully
206 homogenized with a pipette before taking the samples.

207 For determination of nitrogenase activity, filaments grown in BG11 medium were harvested,
208 washed with BG11₀ medium, and resuspended in BG11₀ medium. After 48 h of incubation under growth
209 conditions, the filaments were used in acetylene reduction assays performed under oxic or anoxic
210 conditions at 30°C in the light (ca. 150 $\mu\text{mol photons m}^{-2} \text{ s}^{-1}$). For these assays, the cell suspensions (2 ml,
211 ca. 10 $\mu\text{g Chl ml}^{-1}$) were placed in flasks sealed with rubber stoppers (total volume, 12 to 14 ml). For the
212 anoxic assays, the cell suspensions were supplemented with 10 $\mu\text{M DCMU}$, bubbled thoroughly with
213 argon for 3 min, and incubated for 60 min under assay conditions before starting the reaction. Production
214 of ethylene, determined by gas chromatography in 1-ml samples from the gas phase, was followed for up
215 to three hours after starting the reaction by addition of acetylene (2 ml).

216 **Light, confocal and fluorescence microscopy.** Cultures were routinely observed by light
217 microscopy. To stain the polysaccharide layer of heterocysts, cell suspensions were mixed (1:2) with a
218 filtered 1% (w/v) Alcian Blue (Sigma) solution.

219 For visualization by confocal microscopy of filaments of strains producing genetic fusions to
220 GFP, small blocks of agar-solidified BG11 or BG11₀ medium bearing the filaments were excised and
221 placed in a sample holder with a glass cover slip on top. GFP fluorescence was visualized using a Leica
222 HCX PLAN-APO 63X 1.4 NA oil immersion objective attached to a Leica TCS SP2 confocal laser-
223 scanning microscope. GFP was excited using 488-nm irradiation from an argon ion laser. Fluorescent
224 emission was monitored by collection across windows of 498-541 nm (GFP imaging) and 630-700 nm
225 (cyanobacterial autofluorescence). GFP fluorescence intensity was analyzed using ImageJ 1.45s software.
226 To determine the relative fluorescence intensity in different cell zones, integrated density was recorded in
227 squares of 0.2 to 0.8 μm^2 . About 80 to 190 measurements were made for each of the lateral walls and
228 septal areas of vegetative cells from BG11 or BG11₀ medium, and 50 to 60 measurements were made for
229 lateral walls of heterocysts. We could not accurately quantify GFP fluorescence from heterocyst-
230 vegetative cell septa, which are thinner than the septa between vegetative cells. Because fluorescence did
231 not follow a normal distribution, data are presented as median (*m*) and interquartile ranges (IQR) (40).

232 For fluorescence microscopy, filaments of cells were imaged using a Leica DM6000B

233 fluorescence microscope and an ORCA-ER camera (Hamamatsu). GFP fluorescence was monitored using
234 a FITC L5 filter (excitation BP 480/40, emission BP 527/30) and red autofluorescence was monitored
235 using a Texas Red TX2 filter (excitation BP 560/40, emission BP 645/75).

236 **Immunolocalization of SepJ.** Cells from 1.5 ml of liquid cultures were collected by
237 centrifugation, placed atop a poly-L-lysine pre-coated microscope slide and covered with a 45- μ m pore-
238 size Millipore filter. The filter was removed and the slide was let to dry at room temperature and, then,
239 immersed in 70% ethanol at -20°C for 30 min and dried 15 min at room temperature. The cells were
240 washed twice (2 min each time, room temperature) by covering the slide with PBS-T (PBS supplemented
241 with 0.05% Tween-20). Subsequently, the slides were treated with a blocking buffer (5% milk powder in
242 PBS-T) for 15 min. Cells on the slides were then incubated for 90 min with anti-SepJ-CC antibodies (17)
243 diluted in blocking buffer 1:250, washed three times with PBS-T, incubated 45 min in the dark with anti-
244 rabbit antibody conjugated to fluorescein isothiocyanate (FITC) (Sigma, 1:500 dilution in PBS-T) and
245 washed three times with PBS-T. After dried, several drops of FluorSave (Calbiochem) were added atop,
246 covered with a coverslip and sealed with nail lacquer. Fluorescence was monitored as above, and images
247 were analyzed with ImageJ software (<http://imagej.nih.gov/ij>).

248 **Visualization of nanopores by electron microscopy.** The murein sacculi (which are made of
249 peptidoglycan) were isolated from filaments grown in BG11 medium and analyzed as described
250 previously (18, 19). The purified sacculi were deposited on formvar/carbon film coated copper grids, and
251 stained with 1% (w/v) uranyl acetate. All the samples were examined with a ZEISS LIBRA 120 PLUS
252 electron microscope at 120 kV.

253 **FRAP (fluorescence recovery after photobleaching) analysis.** For assays of intercellular transfer
254 of esculin, filaments were harvested, resuspended in 500 μ l of fresh growth medium, mixed with 15 μ l of
255 saturated (~5 mM) aqueous esculin hydrate solution and incubated for 1 hour in the dark with gentle
256 shaking at 30°C, then washed three times with growth medium, followed by dark incubation for 15 min in
257 1 ml medium at 30°C with gentle shaking. Cells were then washed, spotted onto a BG11 or BG11₀ agar
258 plate (1% w/v), and excess medium was removed. Small blocks of agar with cells adsorbed on the surface

259 were placed in a custom-built temperature-controlled sample holder under a glass cover slip at 30°C
260 except when indicated otherwise. Cells were visualized with a laser-scanning confocal microscope (Leica
261 TCS SP5) using a Leica HCX Plan Apo 63X NA 1.4 oil-immersion objective. Fluorescence was excited
262 at 355 nm, with detection of esculin at 443-490 nm and detection of Chl at 670-720 nm. High-resolution
263 imaging used a 6x line-average with an optical section of ~0.7 µm. FRAP measurements were without
264 line averaging and with a wide pinhole giving an optical section of ~4 µm. After capturing a pre-bleach
265 image, the fluorescence of a defined region of interest was bleached out by scanning this region at ~6x
266 higher laser intensity, and recovery was then recorded in a sequence of full-frame images.

267 For calcein and 5-CF transfer assays, calcein and 5-CF staining and FRAP analysis were
268 performed as previously reported (7, 14). Cell suspensions were spotted onto agar and placed in a custom-
269 built temperature-controlled sample holder with a glass cover slip on top. All measurements were carried
270 out at 30°C. For both calcein and 5-CF, cells were imaged with a Leica HCX PLAN-APO 63X 1.4 NA oil
271 immersion objective attached to a Leica TCS SP5 confocal laser-scanning microscope as previously
272 described for calcein (7) with a 488-nm line argon laser as the excitation source. Fluorescent emission
273 was monitored by collection across windows of 500-520 nm or 500-527 nm in different experiments and
274 a 150-µm pinhole. After an initial image was recorded, the bleach was carried out by an automated FRAP
275 routine which switched the microscope to X-scanning mode, increased the laser intensity by a factor of
276 10, and scanned a line across one cell for 0.137 s before reducing the laser intensity, switching back to
277 XY-imaging mode and recording a sequence of images typically at 1 s intervals.

278 For FRAP data analysis, we quantified kinetics of transfer of the fluorescent tracer either (i) to a
279 terminal cell (with one cell junction) or (ii) a cell somewhere in the middle of a filament (i.e., with two
280 cell junctions). For (i), the recovery rate constant R was calculated from the formula $C_B = C_0 + C_R (1 - e^{-Rt})$, where C_B is fluorescence in the bleached cell, C_0 is fluorescence immediately after the bleach and
281 tending towards $(C_0 + C_R)$ after fluorescence recovery, t is time and R is the recovery rate constant due to
282 transfer of the tracer from one neighbor cell (14). For (ii), the formula $C_B = C_0 + C_R (1 - e^{-2Rt})$ was used.
283 Development of equations for FRAP analysis is described in Supporting information (Text S1).
284

285 **Bacterial Adenylate Cyclase Two-Hybrid (BACTH) strain construction and assays.** The
286 possible interaction of the different glucoside transporters with SepJ was tested using BACTH. For this
287 analysis, all tested genes were amplified using *Anabaena* DNA as template. The following primers were
288 used: alr4781-7 and alr4781-8 to amplify *glsC*; all0261-7 and all0261-8 to amplify *glsP*; and all1711-9
289 and all1711-10 to amplify *hepP*. The PCR products were cloned in vector pSpark I, transformed into *E.*
290 *coli* DH5 α and sequenced. Inserts with the correct sequence were transferred as XbaI- and KpnI-digested
291 fragments to pUT18, pUT18C, pKNT25 and pKT25 producing fusions to the 5' and 3' ends of the genes
292 encoding the adenylate cyclase T18 and T25 fragments, respectively. The resulting plasmids were
293 transformed into *E. coli* XL1-Blue to amplify the plasmids. Fusions of the *sepJ* gene to the 5' end of T18
294 or T25 were as previously described (15). Isolated plasmids were co-transformed into BTH101 (*cya-99*).
295 Transformants were plated onto LB medium containing selective antibiotics and 1% glucose. Efficiencies
296 of interactions between different hybrid proteins were quantified by measurement of β -galactosidase
297 activity in cells from liquid cultures.

298 To determine β -galactosidase activity, bacteria were grown in LB medium in the presence of 0.5
299 mM IPTG and appropriate antibiotics at 30°C for 16 h. Before the assays, cultures were diluted 1:5 into
300 buffer Z (60 mM Na₂HPO₄, 40 mM NaH₂PO₄, 10 mM KCl and 1 mM MgSO₄). To permeabilize cells, 30
301 μ l of toluene and 35 μ l of a 0.1% SDS solution were added to 2.5 ml of bacterial suspension. The tubes
302 were vortexed for 10 s and incubated with shaking at 37°C for 30 min for evaporation of toluene. For the
303 enzymatic reaction, 875 μ l of permeabilized cells were added to buffer Z supplemented with β -
304 mercaptoethanol (25 mM final concentration), to a final volume of 3.375 ml. The tubes were incubated at
305 30°C in a water bath for at least 5 min. The reaction was started by adding 875 μ l of 0.4 mg ml⁻¹ *o*-
306 nitrophenol- β -galactoside (ONPG) in buffer Z. Samples of 1 ml, taken at different times (up to 12 min),
307 were added to 0.5 ml of 1 M Na₂CO₃ to stop the reaction. A_{420 nm} was recorded, and the amount of *o*-
308 nitrophenol produced was calculated using an extinction coefficient $\epsilon_{420 \text{ nm}}=4.5 \text{ mM}^{-1} \text{ cm}^{-1}$ and referred to
309 the amount of total protein, determined by a modified Lowry procedure.

310

311 **RESULTS**

312 **Esculin uptake through α -glucoside transporters.** We have previously shown that esculin can be taken
313 up by *Anabaena* filaments grown in BG11 medium (containing nitrate as the nitrogen source) or grown in
314 BG11 medium and incubated for 18 hours in BG11₀ medium (lacking any source of combined nitrogen),
315 and that uptake is linear for at least 70 min and takes place at higher levels in the filaments incubated in
316 BG11₀ medium (18). To understand better the process of esculin uptake, we determined the dependence
317 of esculin uptake on esculin concentration. Esculin uptake was faster in cells that had been incubated in
318 the absence of nitrate, compared to nitrate-grown cultures, with V_{\max} values of about 0.31 and 0.57 nmol
319 (mg Chl)⁻¹ min⁻¹ for BG11-grown filaments and filaments incubated in BG11₀ medium, respectively (Fig.
320 1). Esculin concentrations giving half-maximal uptake rates (K_s) were 150 and 119 μ M in BG11 and
321 BG11₀, respectively. Because a concentration somewhat lower than the K_s would permit observation of
322 effects such as competitive or non-competitive inhibition, we have used 100 μ M esculin as a standard
323 concentration in our uptake assays.

324 The pH-dependence of uptake of esculin was investigated. As shown in Fig. 2, the rate of uptake
325 was higher at pH 7 than at lower or higher pH values, and was in every case higher in filaments incubated
326 in BG11₀ medium than in filaments from BG11 medium. The difference in the rate of uptake between
327 filaments from BG11₀ and BG11 media decreased as the pH of the assay buffer was increased, suggesting
328 that a H⁺-dependent transporter is induced in filaments incubated in BG11₀ medium.

329 Esculin has been used to test the activity of some higher plant sucrose transporters (41) and,
330 consistent with the possibility of uptake through sucrose transporter(s), inhibition of uptake of esculin by
331 sucrose has been observed in *Anabaena* (18). To characterize further the transporters involved, we tested
332 whether uptake of esculin would be inhibited by various monosaccharides (glucose, fructose, and
333 galactose) and disaccharides (sucrose, maltose, trehalose, and lactose). The results in Fig. 3 show that, in
334 BG11-grown filaments, uptake of esculin is inhibited mainly by sucrose and, to a lesser extent, by

335 maltose. Other sugars tested appear to have stimulated uptake of esculin. In filaments that were incubated
336 in BG11₀ medium, inhibition of uptake by sucrose and maltose was again evident. Our results suggest that
337 although esculin is a β -glucoside, its uptake is inhibited mainly by some α -glucosides, sucrose (glucose
338 $1\alpha \rightarrow 2$ fructose) and maltose (glucose $1\alpha \rightarrow 4$ glucose), whereas neither lactose (a β -galactoside;
339 galactose $1\beta \rightarrow 4$ glucose) nor trehalose (a different α -glucoside; glucose $1\alpha \rightarrow 1\alpha$ glucose) inhibits
340 uptake of esculin.

341 **Identification of three transporters mediating esculin uptake.** Two genes, Ava_2050 and
342 Ava_2748, that encode possible components of ABC uptake transporters for disaccharides or
343 oligosaccharides are induced in the heterocysts of *Anabaena variabilis* ATCC 29413 (42). BLAST
344 analysis with the genomic sequence of *Anabaena* (43) identified Alr4781 and All0261, with 97% and
345 99% amino acid identity, respectively, as the products of the *Anabaena* orthologs of those *A. variabilis*
346 genes. Among characterized proteins included in the Transporter Classification Database (TCDB;
347 <http://www.tcdb.org>), Alr4781 is most similar (45.4% identity, 59.6% similarity; expect, 3.2×10^{-111}) to
348 MalK1, an ATP-binding subunit shared by the glucose/mannose (TCDB no. 3.A.1.1.24) and the
349 trehalose/maltose/sucrose/palatinose (TCDB no. 3.A.1.1.25) transporters from *Thermus thermophilus*,
350 and All0261 is most similar (36.4% identity, 58.9% similarity; expect, 3.3×10^{-51}) to the AraQ permease
351 component of the arabinosaccharide transporter AraNPQ-MsmX from *Bacillus subtilis* (TCDB no.
352 3.A.1.1.34). We denote *alr4781* as *glsC* and *all0261* as *glsP* (*gls* standing for glucoside). Neither *glsC* nor
353 *glsP* is clustered together with other ABC transporter-encoding genes in the *Anabaena* genome. To test
354 whether the transporters encoded by these *Anabaena* genes can be involved in uptake of esculin, *glsC* was
355 inactivated by insertion of gene-cassette C.S3 (44), resulting in *Anabaena* strains that bear the DR3912a
356 mutation (Fig. S1), and *glsP* was inactivated by insertion of C.S3, resulting in *Anabaena* strains that bear
357 the DR3915 mutation, or of C.CE1 (44), resulting in *Anabaena* strains that bear the DR3985a mutation
358 (Fig. S1). BG11-grown filaments of the *glsC* and *glsP* mutants showed esculin uptake activities that were
359 49% and 59% of the wild-type activity, respectively (Table 1), and filaments of the *glsC* and *glsP* mutants

360 that had been incubated in BG11₀ medium showed 74% and 73% of the wild-type activity, respectively.
361 Thus, the products of both genes contribute to esculin uptake by *Anabaena* in medium containing nitrate
362 (BG11) and after incubation in medium lacking combined nitrogen (BG11₀).

363 ABC uptake transporters typically comprise one periplasmic solute-binding protein, two integral
364 membrane proteins (transmembrane domains or permeases) and two nucleotide-binding domains that
365 hydrolyze ATP in the cytoplasm (45). If the GlsC ATP-binding subunit and the GlsP permease belong to
366 the same ABC transporter, we would expect that mutation of the two genes would not increase the effect
367 on the uptake of esculin over that of the single mutations. If, on the other hand, GlsC and GlsP belong to
368 two different transporters, we would expect an additive effect of the mutations. A double *glsC glsP*
369 mutant, i.e., an *Anabaena* strain bearing the DR3912a and DR3985a mutations (Fig. S1), showed 25% of
370 the wild-type activity of esculin uptake in BG11-grown filaments and 50% in filaments incubated in
371 BG11₀ medium (Table 1), percentages that represent decreased values compared to the effects of the
372 single mutations (49% and 59% for BG11 and 74% and 73% for BG11₀). These results suggest that GlsC
373 and GlsP are components of different ABC transporters that can mediate esculin uptake. Notably, a
374 significant uptake activity remains in the double mutant, especially in filaments that had been incubated in
375 medium lacking combined nitrogen (BG11₀).

376 Genes *all1711* (*hepP*) and *alr3705* encode predicted MFS proteins that would facilitate
377 movement of disaccharides or oligosaccharides across cell membranes. As shown by results with mutant
378 *all1711::Tn5-1063*, strain FQ163 (36), HepP may be a glucoside transporter that is involved in production
379 of the heterocyst-specific polysaccharide layer and may also mediate sucrose transport. According to
380 BLAST analysis, Alr3705 is the predicted *Anabaena* genomic product most similar to higher plant
381 sucrose transporters. *alr3705* was mutated by insertion of C.S3-containing plasmid pCSRL49, producing
382 strain CSRL15, and insertion of pCSRL49 was also combined with *all1711::Tn5-1063* to produce a
383 double mutant, strain CSMN3 (Fig. S3). None of strains FQ163, CSRL15, or CSMN3, when grown in
384 BG11 medium, was significantly affected in uptake of esculin (Student's *t* test *P* values 0.553 to 0.703;
385 Table 1), nor was CSRL15 significantly affected when incubated in BG11₀ medium (Table 1). In contrast,

386 filaments of mutants FQ163 and CSMN3 incubated in BG11₀ medium showed similarly decreased
387 activities, 69% and 67% of the wild-type activity, respectively (Table 1). These results indicate that HepP,
388 but not Alr3705, contributed to uptake of esculin in filaments deprived of combined nitrogen.

389 In conclusion, two ABC transporters, of which GlsC and GlsP are independent components, are
390 together responsible for about 75% and 50% of uptake of esculin in BG11- and BG11₀-filaments,
391 respectively, and HepP is responsible for about 30% of uptake of esculin in BG11₀-filaments, when tested
392 at pH 7. Other transporters should therefore contribute to uptake of esculin in both BG11 and BG11₀
393 media.

394 **Subcellular localization of GlsC and GlsP.** To understand better the role of the transporters
395 identified in this work in the physiology of *Anabaena*, we investigated their subcellular localization. The
396 localization of HepP in the cytoplasmic membrane of both vegetative cells and heterocysts has been
397 described previously (36). To study the subcellular localization of GlsC and GlsP, strains producing
398 GlsC-GFP and GlsP-GFP fusion proteins were constructed. As a putative nucleotide-binding domain of
399 an ABC transporter, GlsC is expected to reside in the cytoplasmic face of the cytoplasmic membrane.
400 GlsP is a predicted integral membrane protein that bears six putative transmembrane segments with both
401 the N- and C-termini in the cytoplasm. Because the GFP protein folds efficiently in the cytoplasm (46),
402 the *gfp-mut2* gene was added to the 3' end of the *glsC* and *glsP* genes, and the corresponding constructs
403 were transferred to *Anabaena* (Fig. S4). Visualization of filaments of the corresponding strains, CSMN13
404 (*glsC-gfp*) and CSMN15 (*glsP-gfp*), incubated in BG11 or BG11₀ medium, showed a relatively low GFP
405 signal that was spread through the periphery of the cells including the septal regions, where the signal was
406 increased (Fig. 4). Quantification of GFP fluorescence was performed as described in Materials and
407 Methods and is summarized in Fig. S6. The data show that fluorescence was roughly two-fold higher in
408 the septa than in lateral areas for both GlsC-GFP and GlsP-GFP in cells grown in BG11 medium as well
409 as in cells incubated in BG11₀ medium, indicating that the increased fluorescence from the septa likely
410 corresponds to the combination of the fluorescence from the adjacent cytoplasmic membranes.
411 Nonetheless, somewhat larger GFP fluorescence was observed in septal areas of cells grown in BG11

412 medium than of cells incubated in BG11₀ medium. In filaments incubated in BG11₀ medium, the GFP
413 signal was present at similar levels in heterocysts and vegetative cells. These results indicate that GlsC
414 and GlsP are located throughout the cytoplasmic membrane of both vegetative cells and heterocysts. Our
415 results also indicate that levels of GlsC-GFP or GlsP-GFP are generally similar in cells incubated in
416 BG11 and BG11₀ media (Fig. S6).

417 **Fox phenotype of the *glsC* and *glsP* mutants.** The Fox⁻ phenotype denotes inability to grow
418 fixing N₂ under oxic conditions, and it is frequently associated with malformation of the heterocyst
419 envelope, as in the case of the *hepP* mutant (36). The growth phenotype was here investigated for the
420 *glsC* and *glsP* mutants. On solid medium, the *glsC* and *glsP* single mutants and the *glsC glsP* double
421 mutant could grow using nitrate as the nitrogen source or fixing N₂, but the *glsP* mutant showed poorer
422 diazotrophic growth than the wild type and the *glsC* and *glsC glsP* mutants showed poorer growth in both
423 media (Fig. 5). To determine growth rate constants, growth tests were carried out in liquid medium. In the
424 presence of nitrate (BG11 medium) the growth rate of the single mutants was identical to that of the wild
425 type, whereas the growth rate of the double mutant was 75% that of the wild type (Table 2). In the
426 absence of combined nitrogen (BG11₀ medium), the growth rate of the three mutants was lower than that
427 of the wild type, being especially low in the case of the double mutant (Table 2). Thus, the *glsC*, *glsP* and
428 *glsC glsP* mutants cannot grow normally fixing N₂ under oxic conditions, and therefore show, at best, a
429 weak Fox⁺ phenotype. The phenotype of diminished growth of the single mutants could be complemented
430 by introducing in the corresponding mutant a replicative plasmid bearing the wild-type gene, *glsC* or
431 *glsP*, but, tested on solid medium, complementation was incomplete (Fig. S2). To investigate whether
432 incomplete complementation could result from insufficient expression of the genes in the complemented
433 strains, RT-qPCR analysis was performed as described in Materials and Methods. Rather than low
434 expression, this analysis indicated 6-fold and 11-fold higher expression of the *glsC* and *glsP* genes,
435 respectively, in the complemented mutants than in the wild type. It is possible therefore that
436 overexpression of these genes is deleterious for *Anabaena*.

437 Production of heterocysts and nitrogenase activity were determined in filaments grown in BG11
438 medium and incubated for 48 hours in BG11₀ medium. The *glsC*, *glsP* and *glsC glsP* mutants showed,
439 respectively, about 60%, 85% and 24% the number of heterocysts observed in the wild type (Table 2).
440 Under oxic conditions, nitrogenase activity was about 10% of the wild-type activity in the two single
441 mutants, and about 6.5% in the double mutant (Table 2). Thus, the heterocysts produced in the mutants
442 exhibited low nitrogenase activity. Assay under anoxic conditions showed little or no increase in activity,
443 in contrast to what is normally observed in mutants that bear a defect in the heterocyst envelope (see, for
444 instance, ref. 36). The heterocyst envelope-specific polysaccharide layer can be stained with Alcian Blue,
445 a stain useful to detect bacterial polysaccharides (47). Microscopic inspection of filaments of the *glsC*
446 *glsP* double mutant stained with Alcian Blue showed the presence of stained heterocysts, indicating the
447 existence of a polysaccharide layer in the double mutant (Fig. 6). Microscopic inspection also showed that
448 the filaments of the double mutant were very short (Fig. 6). Inspection of cultures of the three mutants
449 showed the presence of short filaments in the *glsC glsP* double mutant in both BG11 and BG11₀ media,
450 but filament fragmentation was strongest in BG11₀ medium (Fig. S7). Such short filaments were not
451 observed in the *glsC* or *glsP* single mutants. Thus, the phenotypic alterations were stronger in the *glsC*
452 *glsP* double mutant than in the *glsC* or *glsP* single mutants, which is consistent with independent action
453 of the GlcC and GlcP proteins as concluded above from the esculin uptake data.

454 **Intercellular exchange of fluorescent markers.** Because the *glsC*, *glsP*, and *hepP* mutants are
455 impaired in glucoside transport and diazotrophic growth, the proteins encoded by these genes could
456 influence somehow intercellular transfer of sucrose. We therefore tested intercellular exchange of esculin
457 in the *glsC*, *glsP*, and *hepP* mutants by means of FRAP analysis. The results of these tests were analyzed
458 to determine the recovery constant (*R*) of fluorescence in the cells in which esculin had been bleached
459 (see Materials and Methods and Text S1). To attain adequate labeling of esculin to carry out the FRAP
460 analysis, filaments were incubated for one hour with 150 μ M esculin. Transfer of esculin between
461 vegetative cells of BG11-grown filaments was decreased in a limited way (by about 22%) in the *glsC*

462 mutant, although not in the *glsP* mutant (Table 3). However, the effect was larger in the *glsC glsP* double
463 mutant (about 33% inhibition). In the *hepP* mutant, esculin transfer was 43% lower than in the wild type.

464 In filaments of the wild type that had been incubated for 48 h in BG11₀ medium, esculin transfer
465 between vegetative cells was similar to transfer between BG11-grown vegetative cells, but transfer from
466 vegetative cells to heterocysts was decreased to about 38% the value between vegetative cells (Table 3).
467 These results are consistent with previously reported data (18). In the mutants, esculin transfer was lower
468 in the BG11₀-incubated than in the BG11-grown vegetative cells, and it was especially decreased in the
469 *glsC* mutant (Table 3). In contrast, esculin transfer from vegetative cells to heterocysts was increased in
470 all the mutants as compared to the wild type, and this increase was particularly significant in the *hepP*
471 mutant. In summary, esculin transfer was impaired between vegetative cells of heterocyst-containing
472 filaments, but not from vegetative cells to heterocysts.

473 To assess how specific the effect on intercellular transfer could be, transfer of calcein and 5-CF
474 between nitrate-grown vegetative cells was also tested in the mutants. Calcein transfer was significantly
475 impaired in the three single mutants, and it was lowest (21% of the wild-type activity) in the *glsC glsP*
476 double mutant (Table 4). Transfer of 5-CF was also significantly impaired in the *glsC* and *glsP* mutants,
477 although the effect of the mutations was lower in this case than on calcein transfer, and it was not
478 impaired in the *hepP* mutant. These studies showed that GlcC, GlcP, and HepP are required for normal
479 intercellular molecular exchange in *Anabaena*, but this requirement is more evident when the exchange is
480 tested with calcein than with 5-CF or, as shown above, esculin (compare BG11-grown filaments).

481 **SepJ localization and nanopores in the *glsC*, *glsP* and *hepP* mutants.** The fragmentation of
482 filaments observed in the *glsC glsP* double mutant and the effect of the mutation of the glucoside
483 transporters on calcein exchange described above are reminiscent of effects of inactivation of *sepJ* in
484 *Anabaena* (12, 18). We therefore investigated the effect of the inactivation of *glsC*, *glsP* and *hepP* on the
485 subcellular localization of SepJ. For this investigation, plasmids bearing a *sepJ-gfp* fusion gene were
486 transferred to mutants of those genes producing strains CSMN9 (*glsC sepJ-gfp*), CSMN10 (*glsP sepJ-*
487 *gfp*), and CSMN16 (*hepP sepJ-gfp*) (for PCR analysis of the genomic structure of each strain, see Fig.

488 S5). Confocal microscopic inspection of filaments of strains producing SepJ-GFP showed that, whereas
489 the *glsP* and *hepP* mutations did not impair SepJ-GFP localization at the intercellular septa, the *glsC*
490 mutation had a strong effect on localization (Fig. 7; for SepJ-GFP localization in four independent clones
491 inspected by fluorescence microscopy, see Fig. S8). In the *glsC sepJ-gfp* strain, spots of GFP were only
492 sporadically observed in the center of the septa, and the GFP signal was frequently found throughout the
493 periphery of the cells including the intercellular septa. Thus, GlcC, but not GlcP or HepP, appears
494 necessary for proper subcellular localization of SepJ.

495 To corroborate delocalization of SepJ as a result of inactivation of *glsC*, immunolocalization of
496 SepJ was performed using antibodies raised against its coiled-coil domain (17). The antibodies localized
497 SepJ at the cell poles of *Anabaena* (Fig. 8), as previously described (15). In the *glsC* mutant, the signal
498 was largely delocalized, being observed at the cell poles only sporadically. In the complemented strain
499 *glsC-C* (DR3912a [pCSMN22]), SepJ was observed clearly at the cell poles (Fig. 8). These results are
500 fully consistent with the observation that the SepJ-GFP fusion protein shows delocalization of SepJ as the
501 result of inactivation of *glsC* (Figs. 7 and S8).

502 Because SepJ is necessary for *Anabaena* to make a normal number of septal peptidoglycan
503 nanopores (18), the number of nanopores was counted in septal peptidoglycan disks observed in murein
504 sacculi isolated from the wild type and the *glsC*, *glsP* and *hepP* mutants (Fig. 9). Whereas the *glsP* and
505 *hepP* mutants contained a number of nanopores per septum similar to that of the wild type, the septa of
506 the *glsC* mutant contained about 48% of the nanopores found in the wild-type septa.

507 **Protein-protein interactions.** The results in the previous section, showing that GlcC is necessary
508 for proper localization of SepJ and formation of septal peptidoglycan nanopores, provides a rationale for
509 understanding the effect of inactivation of *glsC* on the intercellular transfer of calcein, but no effect of
510 inactivation of *glsP* or *hepP* was found. We then studied possible protein-protein interactions involving
511 the glucoside transporters and SepJ using the BACTH assay, in which adenylate cyclase activity is
512 reconstituted from two fragments, T25 and T18, of an adenylate cyclase from *Bordetella pertussis*
513 brought together by interacting proteins fused to each of those fragments (48). Reconstituted adenylate

514 cyclase in *E. coli* produces cAMP that promotes induction of *lacZ* encoding β -galactosidase. We have
515 previously shown that SepJ-T25 and SepJ-T18 fusions (where the order of protein names denotes N-
516 terminal to C-terminal orientation) are functional in SepJ self-interactions that produce high β -
517 galactosidase activity (15, 16). As is the case for GlsP, HepP is a predicted integral membrane protein
518 with both the N- and C-termini in the cytoplasm (36). Because of possible copy number or steric
519 hindrance problems (49, 50), here we tested possible interactions of SepJ-T25 and SepJ-T18 with both N-
520 terminal and C-terminal fusions to T18 and T25, respectively, of each of the glucoside transporter
521 components investigated in this work, GlsC, GlsP and HepP. The negative control in this analysis is an *E.*
522 *coli* strain carrying plasmids that produce non-fused T25 and T18 fragments, and additional negative
523 controls producing non-fused T25 or T18 and some of the tested fusions were carried out. None of these
524 controls produced β -galactosidase activity significantly different from that of the T25/T18 control (Table
525 5). Combinations of protein fusions involving SepJ that produced β -galactosidase activity significantly
526 higher than the controls included SepJ-T25/SepJ-T18 (positive control), SepJ-T25/T18-HepP, SepJ-
527 T18/T25-HepP and SepJ-T18/T25-GlsP, but no fusion involving GlsC. These results suggest significant
528 interactions between SepJ and GlsP and, more strongly, between SepJ and HepP. On the other hand,
529 significant interactions were also observed between HepP and GlsP. Finally, HepP self-interactions and
530 GlsC self-interactions were also observed suggesting that HepP and GlsC can form homo-oligomers.

531

532 DISCUSSION

533 **Glucoside transporters.** Esculin has been successfully used as a fluorescent analog of sucrose to study
534 intercellular molecular exchange in the filaments of *Anabaena* by means of FRAP analysis (18). This
535 analysis requires esculin to be taken up by the cells in the filament, and we have now identified three
536 genes, *glsC*, *glsP* and *hepP*, that encode components of transporters that mediate esculin uptake in
537 *Anabaena*. The *glsC* (*alr4781*) gene encodes an ATP-binding subunit of an ABC transporter, and the *glsP*
538 (*all0261*) gene encodes an integral membrane (permease) subunit of a different ABC transporter. These

539 genes were investigated because they are the possible *Anabaena* orthologs of genes highly expressed in
540 the heterocysts of a closely related cyanobacterium, *A. variabilis* (42). In *Anabaena*, because the effect of
541 inactivating *glsC* and *glsP* is evident in filaments grown in the presence of nitrate (Table 1), GlcC and
542 GlcP appear to be active in vegetative cells. Additionally, as observed with GFP fusions, GlcC and GlcP
543 are present in heterocysts as well as in vegetative cells (Fig. 4, Fig. S6). In transcriptomic analysis of
544 *Anabaena*, these genes appear to have low expression, and their expression is not affected by nitrogen
545 deprivation (51). According to the results of inhibition of uptake of esculin by sugars (Fig. 3), the natural
546 substrate of these transporters can be sucrose or an α -glucoside. Sucrose uptake by vegetative cells of
547 *Anabaena* has previously been reported (52), and sucrose transporters that can also transport maltose are
548 frequently found in plants (53). The *Anabaena* glucoside transporters could have a role in the recovery of
549 glucosides from extracellular polysaccharides produced under certain physiological conditions, as has
550 been shown to occur in cyanobacterial mats (54). Consistently, biomass of the *glsC* and *glsP* mutants in
551 old BG11 plates is shiny (not shown), which may be indicative of exo-polysaccharide accumulation (36).
552 It is of interest to note also that, although *Anabaena* has been considered an obligatory photoautotroph
553 (28), recent data suggests that it can grow using fructose, albeit this sugar has to be provided at a high
554 concentration unless *Anabaena* is engineered to express a fructose transporter (27, 55). On the other hand,
555 trehalose, lactose, glucose, fructose, and galactose could stimulate esculin uptake (Fig. 3), suggesting that
556 *Anabaena* can use these sugars to support physiological activities such as active transport. As noted
557 earlier, the *Anabaena* genome bears several genes putatively encoding sugar transporters (27), some of
558 which could be involved in the uptake of those sugars.

559 The third gene that encodes an esculin transporter is *hepP* (*all1711*), which encodes an MFS
560 protein that is also necessary for production of the heterocyst-specific polysaccharide layer (36). We have
561 previously shown that HepP is present at higher levels in developing heterocysts (proheterocysts) and
562 heterocysts than in vegetative cells, and that HepP could possibly mediate sucrose uptake specifically in
563 (pro)heterocysts (36). Because the contribution of HepP to uptake of esculin is evident only in filaments
564 that had been incubated in the absence of combined nitrogen, and because uptake of esculin in these

565 filaments is inhibited by sucrose, HepP may be involved in uptake of sucrose/esculin by (pro)heterocysts.
566 MFS proteins including sucrose transporters frequently act as secondary transporters that mediate symport
567 with protons (56). Uptake of esculin that is associated with incubation in BG11₀ medium less uptake in
568 BG11 medium decreases with increasing pH beyond pH 6 (Fig. 2). This observation suggests that a H⁺-
569 dependent transporter is induced in filaments incubated in BG11₀ medium. Because HepP contributes to
570 esculin uptake associated with incubation in BG11₀ medium, our results are consistent with the idea that
571 HepP may be a sucrose-H⁺ or α -glucoside-H⁺ symporter.

572 **Glucoside transporter mutant phenotypes.** Inactivation of *hepP* leads to a Fox⁻ phenotype that
573 has been described in detail (36). We have found that the *glsC* and *glsP* mutants exhibit a weak Fox⁺
574 phenotype: they grow slowly without a source of combined nitrogen under oxic conditions and express
575 low levels of nitrogenase activity (Table 2). Combination in the same strain of the two mutations, *glsC*
576 and *glsP*, resulted in a greater impairment of diazotrophic growth, very low nitrogenase activity and a low
577 percentage of heterocysts. Nonetheless, these heterocysts bore an envelope polysaccharide layer (Fig. 6)
578 and their nitrogenase activity was not substantially increased in anoxic assays, suggesting that they do not
579 have a cell envelope problem. To explore the possibility of a limited sucrose supply to the heterocysts, we
580 investigated whether the *glsC* and *glsP* mutations might affect intercellular molecular exchange tested
581 with the fluorescent sucrose analog esculin. We have observed that the transfer of esculin in filaments of
582 strains mutated in *glsC*, *glsP* or *hepP* is impaired between vegetative cells, but not from vegetative cells
583 to heterocysts (Table 3). Impairment of sucrose transfer between vegetative cells might eventually limit
584 sucrose supply to heterocysts, and a low supply of reductant would explain the low nitrogenase activities
585 detected in *glsC*, *glsP*, and *glsC glsP* mutants. In the case of the *glsC glsP* double mutant, the small
586 number of vegetative cells in heterocyst-containing filaments, which are short (Figs. 6 and S7), may
587 further limit the supply of reductant for nitrogenase. On the other hand, esculin transfer to heterocysts was
588 substantially increased in the *hepP* mutant (Table 3). At least some sucrose transporters of the MFS
589 family can function bidirectionally (56), and this could be the case for HepP that appears to export

590 saccharides from the heterocysts (36). The apparently increased transfer of esculin to heterocysts in the
591 *hepP* mutant might therefore reflect increased retention of esculin in the heterocysts of this strain.

592 **Influence of the glucoside transporters on septal junctions.** Starting from the observation that
593 the *glsC*, *glsP* and *hepP* mutants characterized in this work are impaired in the transfer of esculin between
594 vegetative cells, we found that intercellular transfer of fluorescent markers is in general affected in these
595 mutants, with the highest effect being observed on the transfer of calcein. A greater effect on transfer of
596 calcein than of 5-CF or esculin is reminiscent of the effect of inactivation of *sepJ* (14, 17, 18). Hence,
597 these observations suggest a role of the glucoside transporters in proper function of the SepJ-related septal
598 junctions. GFP fusions indicate that GlcC, GlcP and HepP are located in the periphery of the cells
599 including the intercellular septa (Figs. 4 and S6 and ref. 36), where they could interact with the septal
600 junction complexes. To investigate whether such interactions are feasible, BACTH analysis was carried
601 out with the glucoside transporter proteins and SepJ. This analysis showed that GlcP and, most strongly,
602 HepP can interact with SepJ, whereas no interaction was observed between SepJ and GlcC. Hence, GlcP
603 and HepP may affect SepJ function by means of protein-protein interactions. A functional dependence
604 between SepJ and an ABC transporter for polar amino acids has also been described (57). These
605 observations suggest that proper operation of SepJ, and hence of the SepJ-related septal junctions,
606 requires interaction with other cytoplasmic membrane proteins.

607 GlcC is instead required for proper location of SepJ and maturation of the intercellular septa, as
608 illustrated by the presence of a lower number of nanopores in the *glsC* mutant than in the wild type. How
609 GlcC influences SepJ localization and nanopore formation is unknown, but we note (i) that an N-
610 acetylmuramoyl-L-alanine amidase, AmiC, is required for drilling the septal peptidoglycan nanopores
611 (19) and (ii) that the presence of septal proteins including SepJ is needed for the amidase to make the
612 nanopores (18). In other bacteria, the ABC transporter-like FtsEX complex, in which FtsE is an ATP-
613 binding subunit, is required for activation of amidases that split the septal peptidoglycan during cell
614 division (58, 59) and of endopeptidases that function in cell elongation (60, 61). An appealing hypothesis

615 is that GlsC participates in an ABC transporter-like complex that regulates amidases involved in nanopore
616 formation with an effect on localization of SepJ.

617 The different effects of inactivation of *glsC* –impairment of esculin uptake and alteration of septal
618 structure– indicate that GlsC has multiple functions. Multitask ATP-binding subunits that serve different
619 ABC transporters have been described, e.g., in *Streptomyces lividans* (62), *Streptococcus mutans* (63),
620 *Bacillus subtilis* (64) and *Corynebacterium alkanolyticum* (65), as well as in *Anabaena* (66). As checked
621 at the Integrated Microbial Genomes webpage (<https://img.jgi.doe.gov/cgi-bin/m/main.cgi>), the *glsC* gene
622 is not clustered with any other gene encoding an ABC transporter component in any cyanobacterium
623 whose genome sequence is available. Therefore, no preferential association of GlsC to any particular
624 ABC transporter can be established based on genomic data. Nonetheless, in a few cases the neighboring
625 genes are related to cell wall biosynthesis, including an N-acetylmuramoyl-L-alanine amidase-encoding
626 gene in *Spirulina major* PCC 6313, consistent with the idea of a relation of GlsC to cell wall maturation.

627 In summary, we have identified three genes encoding components of transporters that mediate α -
628 glucoside uptake, including sucrose uptake, in *Anabaena*. These transporters appear to influence septal
629 junction maturation –in the case of *glsC*– or function –in the case of *glsP* and *hepP*. As a consequence,
630 inactivation of these genes impairs molecular transfer between vegetative cells negatively affecting
631 diazotrophy. A major task for future research is to explore whether the interplay between these
632 transporters and SepJ has a function regulating the activity of septal junctions.

633

634 **ACKNOWLEDGMENTS**

635 We thank Antonia Herrero (Sevilla) for useful discussions, Alexandra Johnson (East Lansing)
636 for her cloning work related to generation of DR3912a and DR3915, and Sergio Camargo
637 (Sevilla) for help with the immunofluorescence and RT-qPCR analyses. MN-M was the recipient
638 of a FPU (Formación de Profesorado Universitario) fellowship/contract from the Spanish
639 Government.

640

641 **FUNDING INFORMATION**

642 Work in Seville was supported by grant no. BFU2014-56757-P from Plan Nacional de
643 Investigación, Spain, co-financed by the European Regional Development Fund. Work in East
644 Lansing was supported by the Biosciences Division, Office of Basic Energy Sciences, Office of
645 Science, U.S. Department of Energy (grant DOE FG02-91ER20021).

646

647 REFERENCES

- 648 1. **Flores E, Herrero A.** 2014. The cyanobacteria: morphological diversity in a photoautotrophic
649 lifestyle. *Perspectives in Phycology* **1**:63-72.
- 650 2. **Wolk CP.** 1996. Heterocyst formation. *Annu Rev Genet* **30**:59–78.
- 651 3. **Wolk CP, Ernst A, Elhai J.** 1994. Heterocyst metabolism and development, p 769–823. *In* Bryant
652 DA (ed), *The Molecular Biology of Cyanobacteria*. Kluwer Academic Publishers, Dordrecht.
- 653 4. **Herrero A, Stavans J, Flores E.** 2016. The multicellular nature of filamentous heterocyst-forming
654 cyanobacteria. *FEMS Microbiol Rev* **40**:831-854.
- 655 5. **Flores E, Herrero A, Wolk CP, Maldener I.** 2006. Is the periplasm continuous in filamentous
656 multicellular cyanobacteria? *Trends Microbiol* **14**:439-443.
- 657 6. **Mariscal V, Herrero A, Flores E.** 2007. Continuous periplasm in a filamentous, heterocyst-forming
658 cyanobacterium. *Mol Microbiol* **65**:1139-1145.
- 659 7. **Mullineaux CW, Mariscal V, Nenninger A, Khanum H, Herrero A, Flores E, Adams DG.** 2008.
660 Mechanism of intercellular molecular exchange in heterocyst-forming cyanobacteria. *EMBO J*
661 **27**:1299-1308.
- 662 8. **Mariscal V.** 2014. Cell-cell joining proteins in heterocyst-forming cyanobacteria, p 293-304. *In*
663 Flores E, Herrero A (eds), *The Cell Biology of Cyanobacteria*. Caister Academic Press, Norfolk, UK.
- 664 9. **Mullineaux CW, Nürnberg DJ.** 2014. Tracing the path of a prokaryotic paracrine signal. *Mol*
665 *Microbiol* **94**:1208-1212.
- 666 10. **Flores E, Herrero A, Forchhammer K, Maldener I.** 2016. Septal junctions in filamentous
667 heterocyst-forming cyanobacteria. *Trends Microbiol* **24**:79-82.
- 668 11. **Erickson RO.** 1986. Symplastic growth and symplasmic transport. *Plant Physiol* **82**:1153.
- 669 12. **Flores E, Pernil R, Muro-Pastor AM, Mariscal V, Maldener I, Lechno-Yossef S, Fan Q, Wolk**
670 **CP, Herrero A.** 2007. Septum-localized protein required for filament integrity and diazotrophy in the
671 heterocyst-forming cyanobacterium *Anabaena* sp. strain PCC 7120. *J Bacteriol* **189**:3884-3890.
- 672 13. **Merino-Puerto V, Mariscal V, Mullineaux CW, Herrero A, Flores E.** 2010. Fra proteins
673 influencing filament integrity, diazotrophy and localization of septal protein SepJ in the heterocyst-
674 forming cyanobacterium *Anabaena* sp. *Mol Microbiol* **75**:1159-1170.
- 675 14. **Merino-Puerto V, Schwarz H, Maldener I, Mariscal V, Mullineaux CW, Herrero A, Flores E.**
676 2011. FraC/FraD-dependent intercellular molecular exchange in the filaments of a heterocyst-forming
677 cyanobacterium, *Anabaena* sp. *Mol Microbiol* **82**:87-98.
- 678 15. **Ramos-León F, Mariscal V, Frías JE, Flores E, Herrero A.** 2015. Divisome-dependent subcellular
679 localization of cell-cell joining protein SepJ in the filamentous cyanobacterium *Anabaena*. *Mol*
680 *Microbiol* **96**:566-580.
- 681 16. **Rudolf M, Tetik N, Ramos-León F, Flinner N, Ngo G, Stevanovic M, Burnat M, Pernil R, Flores**
682 **E, Schleiff E.** 2015. The peptidoglycan-binding protein SjcF1 influences septal junction function and
683 channel formation in the filamentous cyanobacterium *Anabaena*. *mBio* **6**(4):e00376-15.
- 684 17. **Mariscal V, Herrero A, Nenninger A, Mullineaux CW, Flores E.** 2011. Functional dissection of
685 the three-domain SepJ protein joining the cells in cyanobacterial trichomes. *Mol Microbiol* **79**:1077-
686 1088.
- 687 18. **Nürnberg DJ, Mariscal V, Bornikoel J, Nieves-Morión M, Krauß N, Herrero A, Maldener I,**
688 **Flores E, Mullineaux CW.** 2015. Intercellular diffusion of a fluorescent sucrose analog via the septal
689 junctions in a filamentous cyanobacterium. *mBio* **6**(2):e02109.

- 690 19. **Lehner J, Berendt S, Dörsam B, Pérez R, Forchhammer K, Maldener I.** 2013. Prokaryotic
691 multicellularity: a nanopore array for bacterial cell communication. *FASEB J* **27**:2293-30.
- 692 20. **Omairi-Nasser A, Mariscal V, Austin JR 2nd, Haselkorn, R.** 2015. Requirement of Fra proteins
693 for communication channels between cells in the filamentous nitrogen-fixing cyanobacterium
694 *Anabaena* sp. PCC 7120. *Proc Natl Acad Sci USA* **112**(32):E4458-E4464.
- 695 21. **Schilling N, Ehrnsperger K.** 1985. Cellular differentiation of sucrose metabolism in *Anabaena*
696 *variabilis*. *Z Naturforsch* **40c**:776-779.
- 697 22. **Curatti L, Flores E, Salerno G.** 2002. Sucrose is involved in the diazotrophic metabolism of the
698 heterocyst-forming cyanobacterium *Anabaena* sp. *FEBS Lett* **513**:175-178.
- 699 23. **López-Igual R, Flores E, Herrero A.** 2010. Inactivation of a heterocyst-specific invertase indicates a
700 principal role of sucrose catabolism in the heterocysts of *Anabaena* sp. *J Bacteriol* **192**:5526–5533.
- 701 24. **Vargas WA, Nishi CN, Giarrocco LE, Salerno GL.** 2011. Differential roles of alkaline/neutral
702 invertases in *Nostoc* sp. PCC 7120: Inv-B isoform is essential for diazotrophic growth. *Planta*
703 **233**:153-162.
- 704 25. **Kolman MA, Nishi CN, Perez-Cenci M, Salerno GL.** 2015. Sucrose in cyanobacteria: from a salt-
705 response molecule to play a key role in nitrogen fixation. *Life (Basel)* **5**:102-126.
- 706 26. **Nieves-Mori6n M, Mullineaux CW, Flores E.** 2017. Molecular diffusion through cyanobacterial
707 septal junctions. *mBio* **8**:e01756-16.
- 708 27. **Stebegg R, Wurzinger B, Mikulic M, Schmetterer G.** 2012. Chemoheterotrophic growth of the
709 cyanobacterium *Anabaena* sp. strain PCC 7120 dependent on a functional cytochrome *c* oxidase. *J*
710 *Bacteriol* **194**:4601-4607.
- 711 28. **Rippka R, Deruelles J, Waterbury JB, Herdman M, Stanier RY.** 1979. Generic assignments,
712 strain histories and properties of pure cultures of cyanobacteria. *J Gen Microbiol* **111**:1-61.
- 713 29. **Hu N-T, Thiel T, Giddings TH, Wolk CP.** 1981. New *Anabaena* and *Nostoc* cyanophages from
714 sewage settling ponds. *Virology* **114**:236–246.
- 715 30. **Mackinney G.** 1941. Absorption of light by chlorophyll solutions. *J Biol Chem* **140**:315-322.
- 716 31. **Ausubel FM, Brent R, Kingston RE, Moore DD, Seidman JG, Smith JA, Struhl K.** 2014. Current
717 *Protocols in Molecular Biology*. Greene Publishing and Wiley-Interscience, New York.
- 718 32. **Elhai J, Vepriiskiy A, Muro-Pastor AM, Flores E, Wolk CP.** 1997. Reduction of conjugal transfer
719 efficiency by three restriction activities of *Anabaena* sp. strain PCC 7120. *J Bacteriol* **179**:1998-2005.
- 720 33. **Cai Y, Wolk CP.** 1990. Use of a conditionally lethal gene in *Anabaena* sp. strain PCC 7120 to select
721 for double recombinants and to entrap insertion sequences. *J Bacteriol* **172**:3138-3145.
- 722 34. **Wolk CP, Cai Y, Cardemil L, Flores E, Hohn B, Murry M, Schmetterer G, Schrautemeier B,**
723 **Wilson R.** 1988. Isolation and complementation of mutants of *Anabaena* sp. strain PCC 7120 unable
724 to grow aerobically on dinitrogen. *J Bacteriol* **170**:1239-1244.
- 725 35. **Valladares A, Rodríguez V, Camargo S, Martínez-Noël GM, Herrero A, Luque I.** 2011. Specific
726 role of the cyanobacterial PipX factor in the heterocysts of *Anabaena* sp. strain PCC 7120. *J Bacteriol*
727 **193**:1172-1182.
- 728 36. **López-Igual R, Lechno-Yossef S, Fan Q, Herrero A, Flores E, Wolk CP.** 2012. A major facilitator
729 superfamily protein, HepP, is involved in formation of the heterocyst envelope polysaccharide in the
730 cyanobacterium *Anabaena* sp. strain PCC 7120. *J Bacteriol* **194**:4677-4687.
- 731 37. **Black TA, Cai Y, Wolk CP.** 1993. Spatial expression and autoregulation of *hetR*, a gene involved in
732 the control of heterocyst development in *Anabaena*. *Mol Microbiol* **9**:77-84 Publisher's correction
733 (1993): *Mol Microbiol* **10**:1153.

- 734 38. Cormack BP, Valdivia RH, Falkow S. 1996. FACS-optimized mutants of the green fluorescent
735 protein (GFP). *Gene* **173**:33-38.
- 736 39. Livak KJ, Schmittgen TD. 2001. Analysis of relative gene expression data using real-time
737 quantitative PCR and the 2(-Delta Delta C(T)) method. *Methods* **25**:402-408.
- 738 40. Krzywinski M, Altman N. 2014. Visualizing samples with box plots. *Nat Methods* **11**:119-120.
- 739 41. Gora PJ, Reinders A, Ward JM. 2012. A novel fluorescent assay for sucrose transporters. *Plant*
740 *Methods* **8**:13.
- 741 42. Park J-J, Lechno-Yossef, S, Wolk CP, Vieille C. 2013. Cell-specific gene expression in *Anabaena*
742 *variabilis* grown phototrophically, mixotrophically and heterotrophically. *BMC Genomics* **14**: 759.
- 743 43. Kaneko T, Nakamura, Y, Wolk CP, Kuritz T, Sasamoto S, Watanabe A, Iriguchi M, Ishikawa
744 A, Kawashima K, Kimura T, Kishida Y, Kohara M, Matsumoto M, Matsuno A, Muraki A,
745 Nakazaki N, Shimpo S, Sugimoto M, Takazawa M, Yamada M, Yasuda M, Tabata S. 2001.
746 Complete genomic sequence of the filamentous nitrogen-fixing cyanobacterium *Anabaena* sp. strain
747 PCC 7120. *DNA Res* **8**:205-213.
- 748 44. Elhai J, Wolk CP. 1988. A versatile class of positive-selection vectors based on the nonviability of
749 palindrome-containing plasmids that allows cloning into long polylinkers. *Gene* **68**:119-138.
- 750 45. Cui J, Davidson AL. 2011. ABC solute importers in bacteria. *Essays Biochem* **50**:85-99.
- 751 46. Drew D, Sjöstrand D, Nilsson J, Urbig T, Chin CN, de Gier JW, von Heijne G. 2002. Rapid
752 topology mapping of *Escherichia coli* inner-membrane proteins by prediction and PhoA/GFP fusion
753 analysis. *Proc Natl Acad Sci USA* **99**:2690-2695.
- 754 47. McKinney RE. 1953. Staining bacterial polysaccharides. *J Bacteriol* **66**:453-454.
- 755 48. Karimova G, Pidoux J, Ullmann A, Ladant D. 1998. A bacterial two-hybrid system based on a
756 reconstituted signal transduction pathway. *Proc Natl Acad Sci USA* **95**:5752-5756.
- 757 49. Battesti A, Bouveret E. 2012. The bacterial two-hybrid system based on adenylate cyclase
758 reconstitution in *Escherichia coli*. *Methods* **58**:325-334.
- 759 50. Stynen B, Tournu H, Tavernier J, Van Dijck P. 2012. Diversity in genetic in vivo methods for
760 protein-protein interaction studies: from the yeast two-hybrid system to the mammalian split-
761 luciferase system. *Microbiol Mol Biol Rev* **76**:331-382.
- 762 51. Flaherty BL, van Nieuwerburgh F, Head SR, Golden JW. 2011. Directional RNA deep
763 sequencing sheds new light on the transcriptional response of *Anabaena* sp. strain PCC 7120 to
764 combined-nitrogen deprivation. *BMC Genomics* **12**:332.
- 765 52. Nicolaisen K, Mariscal V, Bredemeier R, Pernil R, Moslavac S, López-Igual R, Maldener I,
766 Herrero A, Schleiff E, Flores E. 2009. The outer membrane is a permeability barrier for
767 intercellularly exchanged metabolites in a heterocyst-forming cyanobacterium. *Mol Microbiol* **74**:58-
768 70.
- 769 53. Reinders A, Sivitz AB, Ward JM. 2012. Evolution of plant sucrose uptake transporters. *Front Plant*
770 *Sci* **3**:22.
- 771 54. Stuart RK, Mayali X, Lee JZ, Craig Everroad R, Hwang M, Bebout BM, Weber PK, Pett-Ridge
772 J, Thelen MP. 2015. Cyanobacterial reuse of extracellular organic carbon in microbial mats. *ISME J*
773 **10**:1240-1251.
- 774 55. Ungerer JL, Pratte BS, Thiel T. 2008. Regulation of fructose transport and its effect on fructose
775 toxicity in *Anabaena* spp. *J Bacteriol* **190**:8115-8125.
- 776 56. Ayre BG. 2011. Membrane-transport systems for sucrose in relation to whole-plant carbon
777 partitioning. *Mol Plant* **4**:377-394.

- 778 57. Escudero L, Mariscal V, Flores E. 2015. Functional dependence between septal protein SepJ from
779 *Anabaena* sp. strain PCC 7120 and an amino acid ABC-type uptake transporter. *J Bacteriol*
780 **197**:2721-2730.
- 781 58. Yang DC, Peters NT, Parzych KR, Uehara T, Markovski M, Bernhardt TG. 2011. An ATP-
782 binding cassette transporter-like complex governs cell-wall hydrolysis at the bacterial cytokinetic
783 ring. *Proc Natl Acad Sci USA* **108**: E1052-1060.
- 784 59. Bartual SG, Straume D, Stamsås GA, Muñoz IG, Alfonso C, Martínez-Ripoll M, Håvarstein
785 LS, Hermoso JA. 2014. Structural basis of PcsB-mediated cell separation in *Streptococcus*
786 *pneumoniae*. *Nat Commun* **5**: 3842.
- 787 60. Domínguez-Cuevas P, Porcelli I, Daniel RA, Errington J. 2013. Differentiated roles for MreB-
788 actin isologues and autolytic enzymes in *Bacillus subtilis* morphogenesis. *Mol Microbiol* **89**:1084-
789 1098.
- 790 61. Meisner J, Montero Llopis, P, Sham LT, Garner E, Bernhardt TG, Rudner DZ. 2013. FtsEX is
791 required for CwlO peptidoglycan hydrolase activity during cell wall elongation in *Bacillus subtilis*.
792 *Mol Microbiol* **89**:1069-83.
- 793 62. Schlösser A, Kampers T, Schrempf H. 1997. The *Streptomyces* ATP-binding component MsiK
794 assists in cellobiose and maltose transport. *J Bacteriol* **179**:2092-2095.
- 795 63. Webb AJ, Homer KA, Hosie AH. 2008. Two closely related ABC transporters in *Streptococcus*
796 *mutans* are involved in disaccharide and/or oligosaccharide uptake. *J Bacteriol* **190**:168-178.
- 797 64. Ferreira MJ, de Sá-Nogueira I. 2010. A multitask ATPase serving different ABC-type sugar
798 importers in *Bacillus subtilis*. *J Bacteriol* **192**:5312-5318.
- 799 65. Watanabe A, Hiraga K, Suda M, Yukawa H, Inui M. 2015. Functional characterization of
800 *Corynebacterium alkanolyticum* β -xylosidase and xyloside ABC transporter in *Corynebacterium*
801 *glutamicum*. *Appl Environ Microbiol* **81**:4173-4183.
- 802 66. Pernil R, Picossi S, Mariscal V, Herrero A, Flores E. 2008. ABC-type amino acid uptake
803 transporters Bgt and N-II of *Anabaena* sp. strain PCC 7120 share an ATPase subunit and are
804 expressed in vegetative cells and heterocysts. *Mol Microbiol* **67**:1067-1080.

805

806 **Figure legends**

807

808 **Figure 1.** Effect of concentration of esculin on the uptake of esculin by *Anabaena*. BG11-grown
809 filaments or filaments grown in BG11 medium and incubated for 18 h in BG11₀ medium were
810 resuspended in the same media supplemented with 10 mM HEPES-NaOH (pH 7) and used in uptake
811 assays with the indicated concentrations of esculin as described in Materials and Methods. Error bars refer
812 to standard deviations (SD); n = 3.

813 **Figure 2.** Effect of pH on the uptake of esculin by *Anabaena*. Filaments were grown in BG11 medium
814 and were then either resuspended in BG11 medium, or were incubated for 18 h in BG11₀ medium and
815 then resuspended in BG11₀ medium. Both media were supplemented with 10 mM HEPES-NaOH at the
816 indicated values of pH and were used in assays of uptake with 100 μ M esculin as described in Materials
817 and Methods. The differences of the mean values of uptake of esculin between filaments resuspended in
818 BG11₀ and BG11 at the different values of pH tested were represented as BG11₀-BG11. Error bars, SD.
819 For pH 7, n = 25 (BG11) or 20 (BG11₀); for all other values of pH, n = 3.

820 **Figure 3.** Effect of sugars on the uptake of esculin by *Anabaena*. BG11-grown filaments or filaments
821 grown in BG11 medium and incubated for 18 h in BG11₀ medium were resuspended in the same media
822 supplemented with 10 mM HEPES-NaOH (pH 7) and the indicated sugar at 1 mM. No add., no sugar
823 added; Suc, sucrose; Mal, maltose; Tre, trehalose; Lac, lactose; Glc, glucose; Frc, fructose; Gal, galactose.
824 The assays were performed with 100 μ M esculin as described in Materials and Methods. Error bars, SD; n
825 = 2-3, except for No add., 25 (BG11) or 20 (BG11₀). Asterisks denote significant differences in
826 comparison to the assays without added sugars in BG11 or BG11₀ medium (Student's *t* test, *P* < 0.05).

827 **Figure 4.** Subcellular localization of GlcC-GFP and GlcP-GFP. Filaments of strains CSMN13 (*glcC::gfp*)
828 and CSMN15 (*glcP::gfp*) grown in BG11 medium in the presence of antibiotics were incubated in BG11
829 or BG11₀ medium without antibiotics for 24 h. GFP fluorescence was visualized by confocal microscopy

830 as described in Materials and Methods. Brightness and contrast were enhanced to improve visibility.
831 Arrows point to heterocysts. Size bars, 10 μ m.

832 **Figure 5.** Tests of growth on solid medium of wild-type *Anabaena*, and the *glsC* (DR3912a), *glsP*
833 (DR3915), and *glsC glsP* (DR3912a DR3985a) mutants. Filaments grown in BG11 medium (in the
834 presence of antibiotics for the mutants) were resuspended in BG11₀ medium, dilutions were prepared, and
835 a 10- μ l portion of each dilution (from left to right: 1, 0.5, 0.25, 0.125 and 0.0625 μ g Chl ml⁻¹) was spotted
836 on BG11 (NO₃⁻) or BG11₀ (N₂) medium. The plates were incubated under culture conditions, and
837 photographs taken after 7 and 11 days of incubation are shown to help appreciate the growth-defect
838 phenotypes.

839 **Figure 6.** Heterocysts in the *glsC glsP* double mutant. Filaments of the the wild type (PCC 7120) and of
840 the double mutant grown in BG11 medium (in the presence of antibiotics for the mutant) were inoculated
841 in liquid BG11₀ medium without antibiotics and incubated four days under culture conditions. Staining
842 with Alcian Blue was done as described in Materials and Methods, and the filament suspensions were
843 observed by light microscopy. Black arrows point to some stained heterocysts. Scale bars, 10 mm.

844 **Figure 7.** Subcellular localization of SepJ-GFP in the wild-type and transporter mutant genetic
845 backgrounds. Filaments of strains CSAM137 (PCC 7120 [*sepJ::pCSAM137*]), CSMN9 (*glsC::C.S3*
846 *sepJ::pCSVT22*), CSMN10 (*glsP::C.S3 sepJ::pCSVT22*), and CSMN16 (*hepP::Tn1063*
847 *sepJ::pCSAM137*) were grown in BG11 medium in the presence of antibiotics and visualized by confocal
848 microscopy as described in Materials and Methods. Size bars, 10 mm. In the *hepP* mutant SepJ is seen
849 localized in the middle of many cells; these cells are likely starting cell division, and SepJ is known to
850 localize to the cell division site when cell division starts (12, 15).

851 **Figure 8.** Immunofluorescence localization of SepJ in *Anabaena* (PCC 7120) and strains *glsC* and *glsC*-
852 *C*. Filaments of strains PCC 7120, DR3912a (*glsC::C.S3*), and DR3912a [*pCSMN22*] (*glsC::C.S3, glsC*)
853 were grown in BG11 medium in the presence of antibiotics for the mutants and subjected to

854 immunofluorescence analysis with anti SepJ coiled-coil antibodies as described in Materials and Methods.
855 Overlay images of antibody green fluorescence and cyanobacterial autofluorescence are shown. Size bars,
856 10 μ m.

857 **Figure 9.** Septal peptidoglycan disk nanopores in wild-type *Anabaena* and mutants. (A) Murein sacculi
858 were isolated from strains PCC 7120 (WT), DR3912a (*glsC*::C.S3), DR3915 (*glsP*::C.S3) and FQ163
859 (*hepP*::Tn5-1063) grown in BG11 medium and visualized by transmission electron microscopy. (B)
860 Quantification of nanopores in disks from the indicated strains (mean and SD; n, number of disks
861 counted). WT versus *glsC*, Student's *t* test $P = 0.002$.

862

TABLE 1 Esculin uptake in *Anabaena* and some mutant strains.

Strain	Genotype	Product of the mutated gene(s)	Esculin uptake (nmol [mg Chl] ⁻¹ min ⁻¹) ^a			
			BG11		BG11 ₀	
			Mean ± SD (n)	% of WT (P)	Mean ± SD (n)	% of WT (P)
PCC 7120	WT		0.161 ± 0.059 (25)		0.298 ± 0.085 (20)	
DR3912a	<i>alr4781::C.S3</i>	GlsC	0.079 ± 0.037 (10)	49% (0.0003)	0.220 ± 0.065 (9)	74% (0.021)
DR3915	<i>all0261::C.S3</i>	GlsP	0.095 ± 0.041 (10)	59% (0.003)	0.217 ± 0.089 (9)	73% (0.027)
DR3985a- DR3912a	<i>all0261::C.CE</i> <i>alr4781::C.S3</i>	GlsC, GlsP	0.041 ± 0.020 (10)	25% (10 ⁻⁶)	0.149 ± 0.024 (5)	50% (0.007)
CSRL15	<i>alr3705::C.S3</i>	MFS permease	0.181 ± 0.067 (3)	112% (0.591)	0.339 ± 0.073 (4)	113% (0.383)
FQ163	<i>all1711::Tn5-1063</i>	HepP	0.174 ± 0.076 (4)	108% (0.703)	0.206 ± 0.020 (4)	69% (0.046)
CSMN3	<i>alr3705::C.S3</i> <i>all1711::Tn5-1063</i>	MFS permease, HepP	0.139 ± 0.058 (3)	86% (0.553)	0.200 ± 0.042 (4)	67% (0.037)

^a Filaments grown in BG11 medium (in the presence of antibiotics for the mutants) were washed and resuspended in BG11 or BG11₀ media without antibiotics and incubated for 18 h under culture conditions. Filaments were then resuspended in the same media supplemented with 10 mM HEPES-NaOH (pH 7) and used in assays of uptake of 100 μM esculin as described in Materials and Methods. Data are mean and SD of the indicated number of assays performed with independent cultures. Significance of the difference between each mutant and the wild type was assessed by the Student's *t* test; *P* is indicated in each case.

TABLE 2 Growth rates, heterocysts and nitrogenase activity in *Anabaena* and ABC transporter mutant strains.

Strain (mutated genes)	Growth rate constant (μ , day ⁻¹ ; mean \pm SD) ^a		Heterocysts (%) ^b	Nitrogenase activity (nmol ethylene produced [μ g Chl] ⁻¹ h ⁻¹ ; mean \pm SD) ^c	
	BG11	BG11 ₀	48 h -N	Oxic	Anoxic
PCC 7120 (WT)	0.67 \pm 0.07 (5)	0.49 \pm 0.09 (5)	9.33 %	23.37 \pm 5.17 (4)	10.54 \pm 3.05 (3)
DR3912a (<i>glsC</i>)	0.67 \pm 0.14 (5)	0.28 \pm 0.15 (5)	5.58 %	2.52 \pm 1.89 (3)	2.47 \pm 0.15 (2)
DR3915 (<i>glsP</i>)	0.67 \pm 0.07 (5)	0.36 \pm 0.08 (5)	7.93 %	2.13 \pm 0.63 (3)	3.00 \pm 1.48 (2)
DR3912a-DR3985a (<i>glsC glsP</i>) ^d	0.50 \pm 0.10 (5)	0.06 \pm 0.07 (5)	2.22 %	1.53 \pm 1.61 (8)	2.08 \pm 1.70 (6)

^a Growth rate constants were determined in BG11 or BG11₀ liquid media as described in Materials and Methods for the number of independent cultures shown in parenthesis. The difference between the *glsC glsP* mutant and the WT was significant in BG11 (Student's *t* test *P* = 0.014) and BG11₀ (*P* < 0.001) media; the differences were also significant between *glsC* and WT (*P* = 0.029) and between *glsP* and WT (*P* = 0.045) in BG11₀ medium.

^b Filaments of the indicated strains grown in BG11 medium (with antibiotics for the mutants) and incubated in BG11₀ medium without antibiotics for 48 h were used to determine the percentage of heterocysts (about 1,500 cells counted for each strain).

^c Filaments of the indicated strains grown in BG11 medium (with antibiotics for the mutants) and incubated in BG11₀ medium without antibiotics for 48 h were used to determine nitrogenase activity. Acetylene reduction was assayed under oxic and anoxic conditions (see Materials and Methods); the differences were significant for all the mutants vs. the WT (Student's *t* test *P* < 0.002 [oxic conditions] and \leq 0.05 [anoxic conditions]). The number of determinations done with independent cultures is indicated in parenthesis.

^d After 48 h of incubation in BG11₀ medium, the filaments of this strain were extensively fragmented (see the text). Those filaments containing heterocysts also contained a mean of 5.4 vegetative cells per filament.

TABLE 3 Transfer of esculin between vegetative cells or from vegetative cells to heterocysts in *Anabaena* and glucoside transporter mutant strains.

Strain (mutated genes)	Esculin transfer (R , s ⁻¹) ^a					
	BG11-grown filaments		Filaments incubated in BG11 ₀ medium			
	Vegetative cells		Vegetative cells		Heterocysts	
	Mean \pm SD (n)	% of WT (P)	Mean \pm SD (n)	% of WT (P)	Mean \pm SD (n)	% of WT (P)
PCC 7120 (WT)	0.157 \pm 0.052 (49)		0.162 \pm 0.062 (60)		0.060 \pm 0.067 (82)	
DR3912a (<i>glsC</i>)	0.122 \pm 0.051 (77)	78% ($< 10^{-3}$)	0.047 \pm 0.048 (28)	29% ($< 10^{-12}$)	0.074 \pm 0.081 (55)	123% (0.277)
DR3915 (<i>glsP</i>)	0.144 \pm 0.054 (43)	92% (0.200)	0.094 \pm 0.077 (25)	58% ($< 10^{-4}$)	0.091 \pm 0.084 (33)	152% (0.060)
DR3912a, DR3985a (<i>glsC glsP</i>)	0.105 \pm 0.042 (55)	67% ($< 10^{-6}$)	0.094 \pm 0.070 (37)	58% ($< 10^{-5}$)	0.088 \pm 0.057 (25)	147% (0.070)
FQ163 (<i>hepP</i>)	0.090 \pm 0.058 (56)	57% ($< 10^{-4}$)	0.068 \pm 0.051 (17)	42% ($< 10^{-10}$)	0.156 \pm 0.082 (27)	260% (10^{-8})

^a Filaments of the wild type and the indicated mutants grown in BG11 medium (with antibiotics for the mutants) and incubated in BG11 medium without antibiotics for 18 to 24 h or in BG11₀ medium without antibiotics for 48 h were used in FRAP analysis as described in Materials and methods. Data are mean \pm SD from the results obtained with the indicated number of filaments (n) subjected to FRAP analysis. Filaments from two to six independent cultures were used. Student's *t* test (mutant vs. wild type) *P* is indicated in each case.

Table 4 Transfer of calcein and 5-CF between nitrate-grown vegetative cells in *Anabaena* and glucoside transporter mutant strains^a.

Strain (mutated genes)	Calcein transfer (R , s ⁻¹)		5-CF transfer (R , s ⁻¹)	
	Mean \pm SD (n)	% of WT (P)	Mean \pm SD (n)	% of WT (P)
PCC 7120 (WT)	0.070 \pm 0.053 (50)		0.087 \pm 0.045 (136)	
DR3912a (<i>glsC</i>)	0.039 \pm 0.033 (47)	55% ($< 10^{-3}$)	0.069 \pm 0.060 (105)	79% (0.009)
DR3915 (<i>glsP</i>)	0.028 \pm 0.041 (68)	39% ($< 10^{-5}$)	0.059 \pm 0.059 (96)	68% ($< 10^{-4}$)
DR3912a, DR3985a (<i>glsC glsP</i>)	0.015 \pm 0.020 (43)	21% ($< 10^{-8}$)	0.064 \pm 0.054 (48)	74% (0.004)
FQ163 (<i>hepP</i>)	0.022 \pm 0.027 (33)	31% ($< 10^{-5}$)	0.082 \pm 0.044 (27)	94% (0.604)

^a Filaments of the wild type and the indicated mutants grown in BG11 medium (with antibiotics for the mutants) and incubated in BG11 medium without antibiotics for 18 to 24 h were used in FRAP analysis as described in Materials and Methods. Data are mean \pm SD from the results obtained with the indicated number of filaments (n) subjected to FRAP analysis. Filaments from two to six (calcein) or up to 9 (5-CF) independent cultures were used. Student's t test (mutant vs. wild type) P is indicated in each case.

Table 5 Bacterial two-hybrid analysis of protein-protein interactions^a.

	<i>T18</i>	<i>SepJ-T18</i>	<i>GlsC-T18</i>	<i>T18-GlsC</i>	<i>GlsP-T18</i>	<i>T18-GlsP</i>	<i>HepP-T18</i>	<i>T18-HepP</i>
<i>T25</i>	12.66 ± 2.34 (9)	10.88 ± 1.06 (6)	13.01 ± 3.49 (4)	12.34 ± 0.80 (4)	12.11 ± 4.10 (4)	10.95 ± 3.37 (4)	12.12 ± 1.33 (4)	11.99 ± 2.69 (4)
<i>SepJ-T25</i>	11.22 ± 2.04 (2)	** 80.12 ± 37.03 (9)	13.25 ± 2.91 (5)	15.75 ± 11.31 (3)	11.74 ± 3.68 (5)	14.66 ± 2.12 (4)	11.42 ± 1.36 (4)	** 28.35 ± 5.93 (4)
<i>GlsC-T25</i>	Nd	11.66 ± 1.99 (6)	12.52 ± 3.32 (4)	* 20.52 ± 4.90 (4)	12.36 ± 0.95 (3)	13 ± 5.72 (3)	12.27 ± 3.61 (3)	12.11 ± 1.48 (4)
<i>T25-GlsC</i>	Nd	13.09 ± 3.06 (6)	** 25.98 ± 5.46 (4)	15.93 ± 6.35 (6)	12.72 ± 3.11 (4)	12.79 ± 3.73 (3)	13.57 ± 1.92 (4)	11.98 ± 0.86 (4)
<i>GlsP-T25</i>	Nd	14.34 ± 2.22 (7)	12.32 ± 3.11 (5)	14.19 ± 7.44 (4)	12.16 ± 2.11 (4)	11.64 ± 4.06 (3)	13.13 ± 2.23 (4)	17.44 ± 4.70 (4)
<i>T25-GlsP</i>	Nd	** 29.12 ± 9.36 (7)	11.80 ± 2.27 (5)	15.48 ± 8.28 (4)	11.85 ± 0.55 (3)	12.04 ± 6.11 (3)	13.63 ± 1.47 (4)	* 23.08 ± 7.03 (4)
<i>HepP-T25</i>	10.58 ± 4.35 (4)	12.96 ± 3.26 (4)	12.83 ± 1.50 (4)	12.08 ± 1.12 (4)	13.94 ± 2.29 (4)	13.65 ± 2.48 (4)	13.86 ± 1.37 (4)	16.73 ± 8.38 (4)
<i>T25-HepP</i>	13.60 ± 2.01 (4)	** 75.31 ± 6.74 (4)	14.56 ± 2.47 (4)	13.06 ± 2.81 (4)	18.33 ± 2.50 (4)	** 34.16 ± 7.18 (4)	13.77 ± 0.99 (4)	** 79.97 ± 22.12 (4)

^a Interactions of T25- and T18-fusion proteins produced in *E. coli* were measured as β -galactosidase activity in liquid cultures. Activity corresponds to nmol *o*-nitrophenol (mg protein)⁻¹ min⁻¹. The protein fused to the N- or the C-terminus of T18 or T25 is indicated in each case (N-terminus, protein-T18 or protein-T25; C-terminus, T18-protein or T25-protein). The mean and standard deviation of the results obtained with the indicated number of independent transformants (n) is presented. The difference between each fusion protein combination and the T18/T25 pair was assessed by the Student's *t* test; bold type denotes significant differences (*, $P \leq 0.005$; **, $P \leq 0.001$). All other combinations gave activities not significantly different from the T25/T18 control, $P > 0.05$. Nd, not determined.

Fig. 1

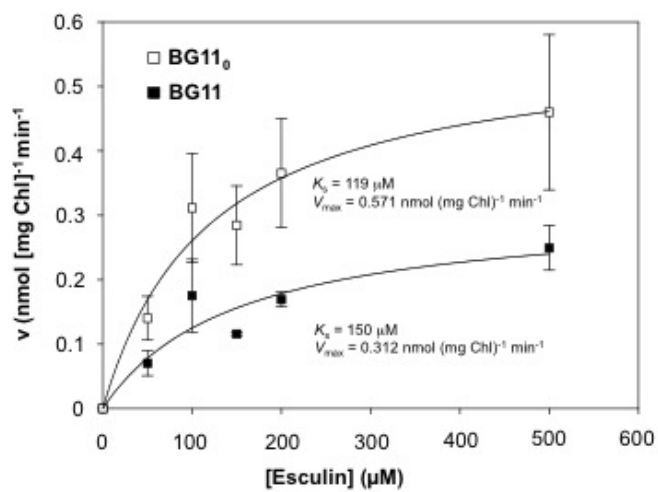


Fig. 2

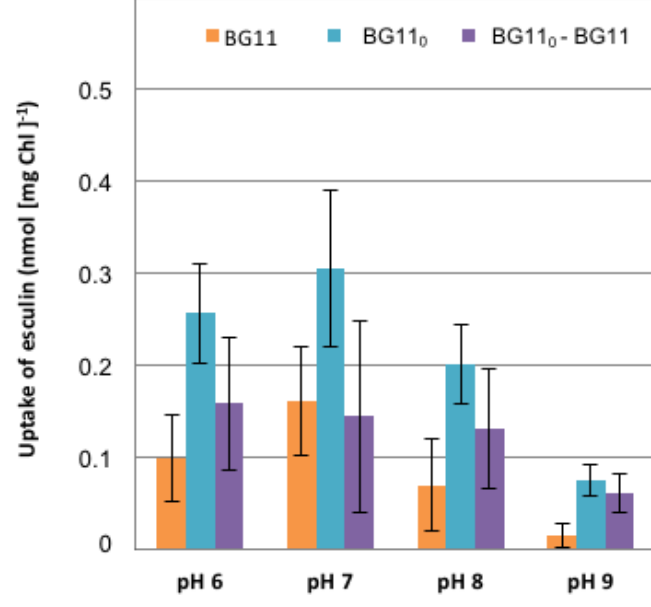


Fig. 3

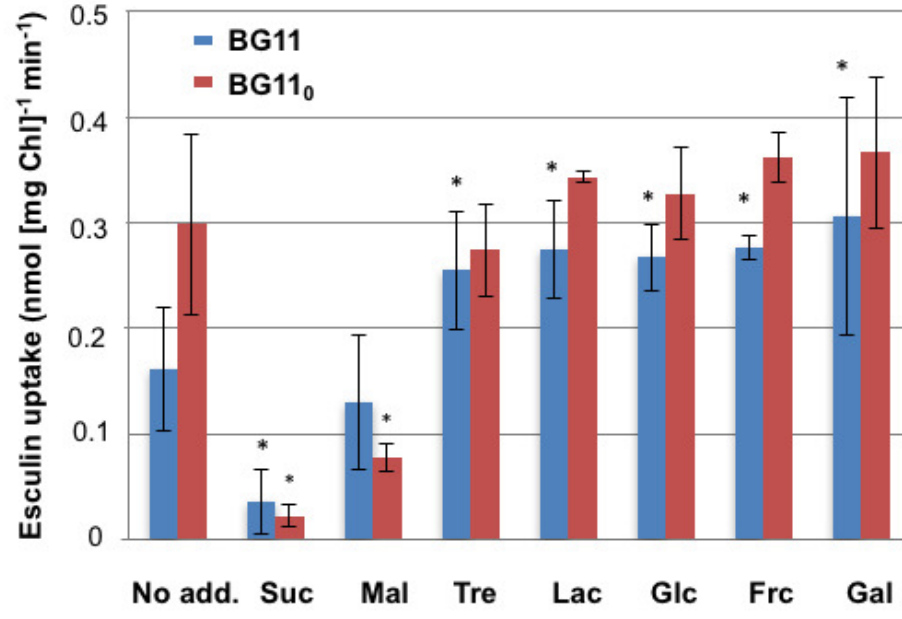


Fig. 4

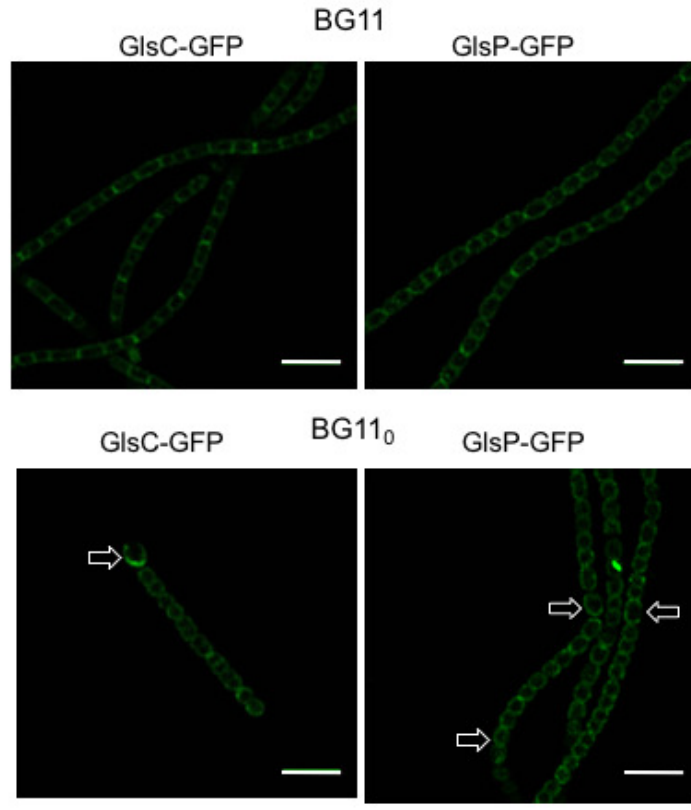


Fig. 5

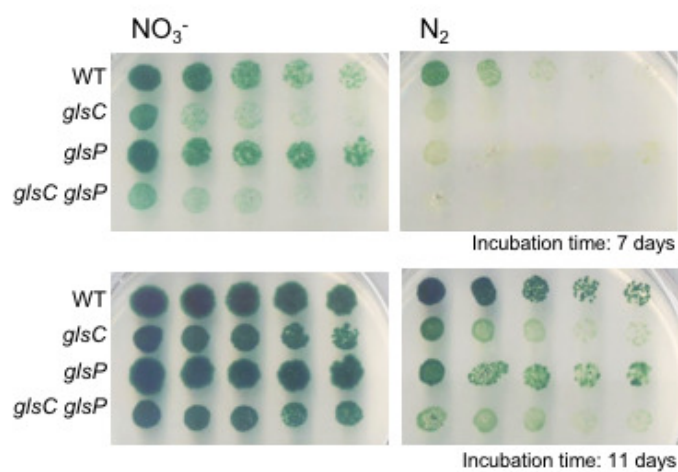


Fig. 6

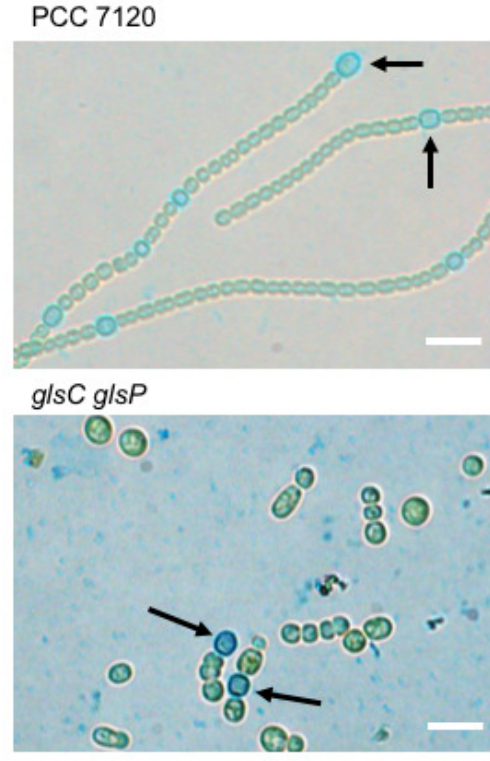


Fig. 7

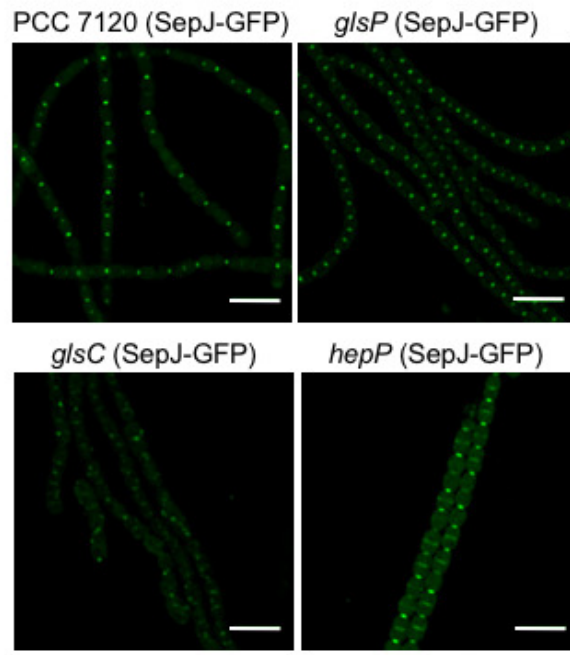


Fig. 8

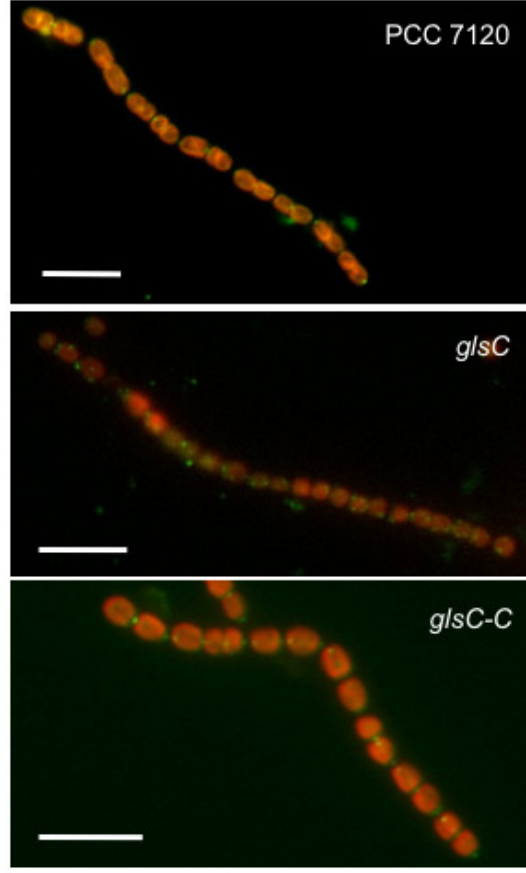


Fig. 9

